IEEE Access
Multidisciplinary ⋮ Rapid Review ⋮ Open Access Journal

Received 28 July 2023, accepted 22 August 2023, date of publication 28 August 2023, date of current version 7 September 2023.

Digital Object Identifier 10.1109/ACCESS.2023.3309300

TOPICAL REVIEW

Measurement Techniques and Challenges of Wireless LC Resonant Sensors: A Review

MEHEDI MASUD[1], PATRICIA VAZQUEZ[1], MUHAMMAD RIAZ UR REHMAN[1], (Graduate Student Member, IEEE), ADNAN ELAHI[2], WILLIAM WIJNS[1], AND ATIF SHAHZAD[1,3]

[1]Smart Sensors Laboratory, The Lambe Institute for Translational Medicine and Curam, College of Medicine, Nursing and Health Sciences, University of Galway, Galway, H91 TK33 Ireland
[2]Department of Electrical and Electronic Engineering, School of Engineering, University of Galway, Galway, H91 TK33 Ireland
[3]Centre for Systems Modelling and Quantitative Biomedicine (SMQB), University of Birmingham, B15 2TT Birmingham, U.K.

Corresponding author: William Wijns (william.wyns@universityofgalway.ie)

This work was supported in part by the Department of Enterprise, Trade and Employment and Enterprise Ireland Disruptive Technology Innovation Fund under Grant DT20200210A; in part by the Science Foundation Ireland Research Professorship under Grant 15/RP/2765; and in part by the University of Birmingham Dynamic Investment Fund.

ABSTRACT Wireless operation of *LC* resonant sensors is based on magnetic coupling between two inductive coils, where the inductor of the sensor acts as a secondary coil for the magnetic coupling. An external reader coil is used as a primary coil to interrogate the sensor and detect the sensor's response. Wireless *LC* resonant sensors are used in many applications where cable connections for powering the sensor and acquiring its response are inconvenient. This review focuses on the fundamental operating principles of wireless *LC* resonant sensors, their measurement techniques and challenges, as well as potential solutions. The main challenge in wireless measurement of the sensors is to accurately measure the resonance frequency and the quality factor of the sensor, which are solely dependent on the intrinsic parameters of the sensors. For practical wireless applications, it is crucial to interrogate *LC* resonant sensors regardless of their wireless measurement distances. To interrogate the wireless resonant sensor, frequency and time domain measurements are commonly used. The coupling coefficient, which is greatly influenced by the geometrical dimensions and alignment of the two inductively coupled coils, has an adverse effect on distance independent measurement of the sensors in frequency domain phase dip technique. Furthermore, the presence of parasitic capacitance that appears in parallel to the readout coil of the sensor has also an adverse effect on distance independent measurement in both the frequency and time domains, resulting in an inaccurate measurement of the sensors' resonance frequency. A parasitic capacitance compensation technique can be employed to reduce or even eliminate the presence of parasitic capacitance in the readout coil, which significantly improves the measurement accuracy of the *LC* resonant sensors.

INDEX TERMS *LC*, wireless, resonant sensor, frequency domain, time domain, distance independent measurement.

I. INTRODUCTION

The concept of wireless sensing gained significant attention after the introduction of ''endo-radiosonde'' in 1957, which is a smart capsule comprised of a transducer and radio transmitter that can be swallowed as a pill to monitor gastrointestinal pressure and wirelessly transmit the pressure value to the outside of the human body [1]. Collins published a pioneering work in 1967 on a miniaturised implantable 'transensor' based on a wireless resonant circuit for continuously monitoring intraocular pressure in rabbit eyes [2]. Subsequently, numerous studies were devoted to the design, fabrication, and experimental characterization of various or other resonant sensor topologies to measure a variety of physical parameters, including pressure, temperature, humidity, biochemical species, gas, and more [3], [4], [5], [6], [7], [8], [9],

The associate editor coordinating the review of this manuscript and approving it for publication was Santosh Kumar.

[10]. Wireless sensing of physical or biometric parameters of interest is advantageous for applications where cable connections are difficult or challenging to establish. In biomedical implants, for example, transcutaneous wires branching off the skin increase the risk of infection for short or long-term monitoring of the physiological parameters, compromising the patient's safety and comfort [11]. In practice, wireless sensors can be categorised into two groups: active and passive sensors.

Active sensors typically have signal processing and wide wireless data transmission capability, which complicates sensor configuration and necessitates active power supply, making them unsuitable for implants and applications in harsh environments [12], [13], [14], [15]. Wireless passive sensors, on the other hand, are composed of passive elements–such as resistor, inductor, and capacitor –that only participate in data transmission and hence do not require an active power supply [16], [17], [18]. Passive sensors are therefore suitable for applications where cable connections are challenging, but their use necessitates a sophisticated reader system. Some active/semi-passive wireless sensors include batteries or energy harvesting capabilities: however, batteries must be replaced periodically, and low densities of scavenged energy and low conversion efficiency of the energy harvester make the passive operation of the resonant sensors–such as *LC*–more appealing for wireless measurements [19], [20], [21]. For example, recent commercial success in wireless *LC* sensing technology is EndoSure Wireless AAA pressure sensor and ImPressure AAA Sac Pressure Sensor by CardioMems and Remon Medical Technologies, respectively [22], [23]. Endotronix, Inc.'s *LC* based pressure sensor has also recently been investigated in human trials for Pulmonary Artery Pressure sensing with the Cordella Heart Failure System [24], [25].

Two measurement techniques, frequency and time domain, are widely applied to extract the resonance frequency and quality factor of a resonant sensor [26]. Frequency domain measurement is performed with either a bulky and expensive vector network analyser (VNA)/impedance analyser (IA) or custom designed front-end electronics with complex functionality to measure the reflection coefficients or the equivalent impedance of the sensors [27], [28], [29], [30], [31], [32]. One of the frequency domain measurement techniques is phase dip which measures the phase of the equivalent impedance, and shows a dip in phase at resonant frequency of the sensors [33], [34], [35].

Despite having a wide dynamic range and better signal to noise ratio (SNR), the phase dip measurement technique is dependent on coupling coefficient k, and requires a fixed wireless interrogation distance between the sensor and reader systems which is not suitable for wireless measurement of the sensors. Nopper et al. showed that instead of measuring the phase, the measurement of the real part of equivalent impedance does not have a dependence on the k and hence, the wireless measurement distance [36], [37]. On the other hand, time domain measurement of the sensor utilises the damped decay response to extract the resonance frequency and quality factor of the sensors [38], [39]. Analytical modeling of the *LC* resonant sensors in the time domain shows that the resonance frequency is independent of the wireless interrogation distance. However, Demori et al. showed that measurement of the real part of equivalent impedance in the frequency domain and damped decay response in the time domain both suffer from undesired distance dependent measurement of *LC* sensors [64]. It is due to the fact that non avoidable parasitic capacitance appears in parallel to the readout coil of the sensors.

Although there has been significant progress in *LC* sensor design and its applications, literature reporting the commonly practiced measurement techniques on the *LC* resonant sensors is sparse. Li et al. published a review on *LC* resonant sensors for harsh environmental applications which briefly covers the phase dip measurement techniques in the frequency domain [40]. Recently, Bhar et al. reported on the advancement of wireless *LC* sensors for temperature measurement which includes sensor design principles, sensor fabrication technologies, and materials [41]. Huang et al. covered a great deal of basic components of the sensors, sensing mechanisms, and measurement techniques both in time and frequency domain [42]. Not analyzed so far is the recent recognition of the effect of parasitic capacitance, which appears in parallel to the readout coil, resulting in inaccurate distance dependent measurement of the sensors in both time and frequency domain.

Therefore, this review covers the gap of recent developments on the measurement challenges of wireless *LC* resonant sensors by providing a comprehensive update on the state-of-the-art and the background theory on the measurement techniques along with numerical simulations. Section (II) provides the background theory of the basic components of the sensors. Measurement techniques for both frequency and time domain are discussed in section (III) by providing analytical modeling, numerical simulation, and examples from experimental results. Wireless sensor measurement challenges are discussed in section (IV) by covering the effects on the presence of parasitic capacitance which appears in parallel to the readout coil, resulting distance dependent measurement of the sensors. Furthermore, section (V) covers the recently reported parasitic capacitance compensation technique which ceases the dependance of the parasitic capacitance for distance independent measurement of the sensor. Other sensor prospects and related discussions are covered in section (VI). The final section offers concluding remarks in (VII). And a flowchart representing in Fig. 1 gives the gist of the paper.

II. BASIC COMPONENTS OF LC SENSORS

An *LC* resonant sensor consists with basic electrical elements inductor L, and capacitor C, where either of them can be used as a sensing element of the sensor. The majority of *LC*

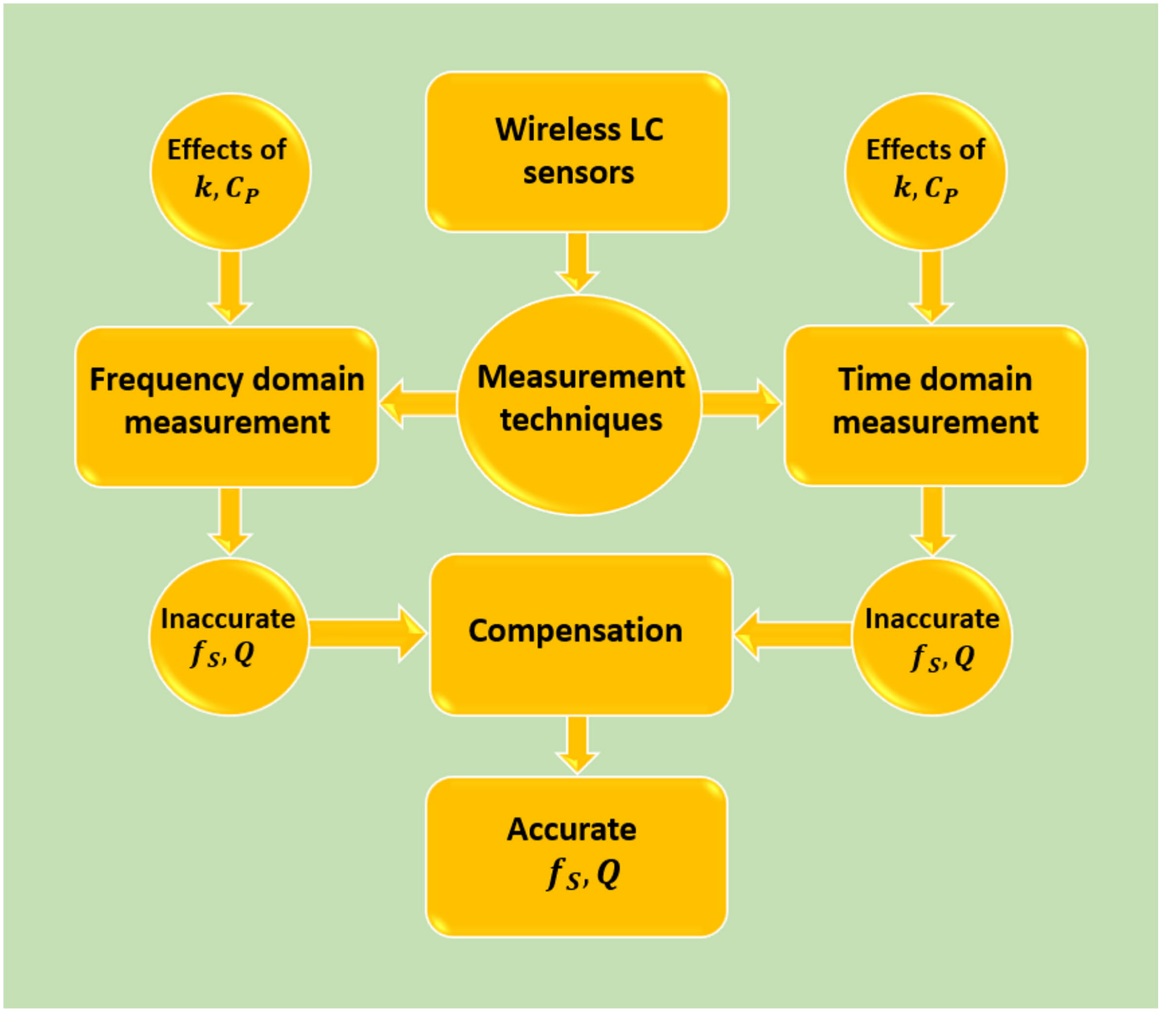

FIGURE 1. Block diagram representation of measurement techniques and challenges of wireless *LC* resonant sensors.

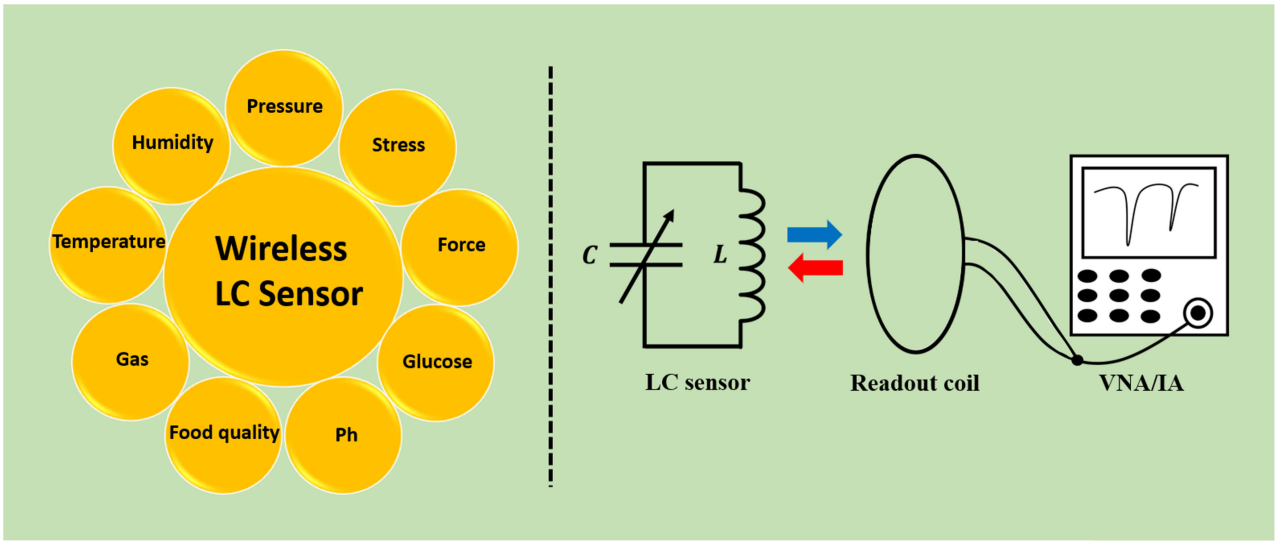

FIGURE 2. Typical schematic representation of the measurement of wireless *LC* resonant sensor by Vector Network Analyser (VNA)/ Impedance Analyser (IA) to measure different physical parameters.

resonant sensors' sensing element is capacitive. The change of capacitance in response to the measurand of interest shifts the resonant frequency of the *LC* sensor. Much research is being conducted to improve the sensing capability of the

sensing elements–capacitive sensor–in terms of performance, fabrication, and cost-effectiveness. As a result, new sensor designs and the search for new dielectric materials are unavoidable in order to address the unmet challenges.

A. INDUCTOR

To optimise the inductive coil for wireless interrogation of the *LC* sensors, various design topologies have been investigated. Sensor coils are typically designed using solenoid and planner spiral inductors. Fig. 3. (a) and 3. (b) show schematic representations of a planar square shape spiral inductor and a solenoid inductor coil, respectively. Despite having a lower quality factor, the inductance of the planar spiral inductor is well-defined over a wide range of process variations and widely used in electronics. Because of their simpler layout, square spiral inductors are more popular than hexagonal, octagonal, and circular inductors. Furthermore, apart from using the inductive coil for electromagnetic coupling, it is also possible to make inductive coil as a sensing element of the sensors [43], [44], [45], [46]. An inductive coil can be completely specified for a given shape as follows: number of turns n, turn width w, turn spacing s, outer diameter d_{out}, inner diameter d_{in}, average diameter $d_{\text{avg}} = (d_{\text{out}} + d_{in})/2$ and fill ratio is defined as $\rho = (d_{\text{out}} - d_{\text{in}})/(d_{\text{out}} + d_{\text{in}})$ [47], [78]. For the discrete inductor, Wheeler developed several formulas for a planar spiral inductive coil. The inductance for a planar spiral inductor can be obtained using a straightforward modification of the original Wheeler formula as follows [48]:

$$L = K_1 \mu \frac{n^2 d_{\text{avg}}}{1 + K_2 \rho} \tag{1}$$

where ρ is the fill ratio, d_{avg} is the average diameter, $\mu = \mu_0 \mu_r$ is the proportionality magnetic permeability, which is the product of the permeability of the free space μ_0, and μ_r is the permeability of the specific medium, K_1 and K_2 are layout dependent parameters with different values for square, hexagonal, and octagonal shapes. On the other hand, the inductance of the solenoid coil with a given length l, cross-sectional area A, and the number of turns N can be calculated by the basic physical law of electromagnetics as follows:

$$L = \frac{\mu N^2 A}{l} \tag{2}$$

B. CAPACITOR

Capacitive sensors are commonly used as a sensing element of wireless *LC* resonant sensors in many applications [49], [50], [51], [52]. Among various capacitive sensing topologies, parallel plate and interdigitated capacitors are widely implemented for practical applications, as shown in Fig. 3. (c), and 3. (d), respectively. A parallel plate capacitive sensor is typically designed by implementing the fundamental formula of the capacitance, which can be expressed as:

$$C = \frac{\varepsilon_0 \varepsilon_r A}{d} \tag{3}$$

where $\varepsilon_0 = 8.85 \times 10^{-12}$ F/m is the permittivity of free space, ε_r is the relative permittivity of dielectric, A is the surface area of the plates, and d is the separation gap between the two plates. On the other hand, the total capacitance of the interdigitated capacitor is calculated by the following formula [53]:

$$C_{\text{total}} = C_{uc}(N-1)L_l \tag{4}$$

where N is the number of unit cells of the capacitor, L_l is the length of the electrode fingers, and C_{uc} is the unit cell capacitance per length and can be written as:

$$C_{uc} = \varepsilon_0 (\varepsilon_r + \varepsilon_k) \frac{K_1\left(\sqrt{1 - \left(\frac{a}{b}\right)^2}\right)}{K_1\left(\frac{a}{b}\right)} + 2\varepsilon_0 \varepsilon_k \frac{t}{a} \tag{5}$$

where ε_0 is the vacuum permittivity, ε_r is the dielectric constant of the substrate, ε_k is the dielectric constant of the dielectric film, K_1 is the complete elliptic integral of the first kind, t is the electrode thickness, a is the electrode's width, b is the distance between fingers.

C. LC RESONANT CIRCUIT

An *LC* resonant tank circuit, as shown in Fig. 3. (e), can be used to derive the electric equivalent *LC* resonant sensor. However, the internal structure of the *LC* sensor is basically an *RLC* circuit where the resistive component R appears from the equivalent series resistance of the inductive coil L and the capacitor C, and hence *LC* sensors are often referred to as *RLC* sensors as shown in Fig. 3. (f). The analytical expression for *RLC* resonant circuit under the excitation source shown in Fig. 3. (g) in Laplace domain for complex frequency $s = j\omega$ can be derived as follows by applying Kirchhoff's Voltage Law (KVL) [54]:

$$V(S) = I(S)\left(R + sL + \frac{1}{sC}\right) \tag{6}$$

The impedance of the *RLC* circuit can be written as follows after rearranging equation (6):

$$Z(S) = \frac{V(S)}{I(S)} = R + sL + \frac{1}{sC} = \frac{s^2 LC + sCR + 1}{sC} \tag{7}$$

Under the resonance condition, the energy supplied to the *RLC* resonant circuit will oscillate between the capacitor and the inductor, and the impedance $Z(S)$ will be at it's minimum. Therefore, the equation (7) can be expressed as follows by setting $Z = 0$:

$$s^2 + s\frac{R}{L} + \frac{1}{LC} = 0 \tag{8}$$

which is a quadratic equation and its roots are as follows:

$$s_{1,2} = -\frac{R}{2L} \pm \sqrt{\left(\frac{R}{2L}\right)^2 - \frac{1}{LC}} \tag{9}$$

The response the *RLC* circuit will be overdamped, critically damped, and underdamped,for $\frac{R}{2L} > \frac{1}{\sqrt{LC}}$, $\frac{R}{2L} = \frac{1}{\sqrt{LC}}$ and

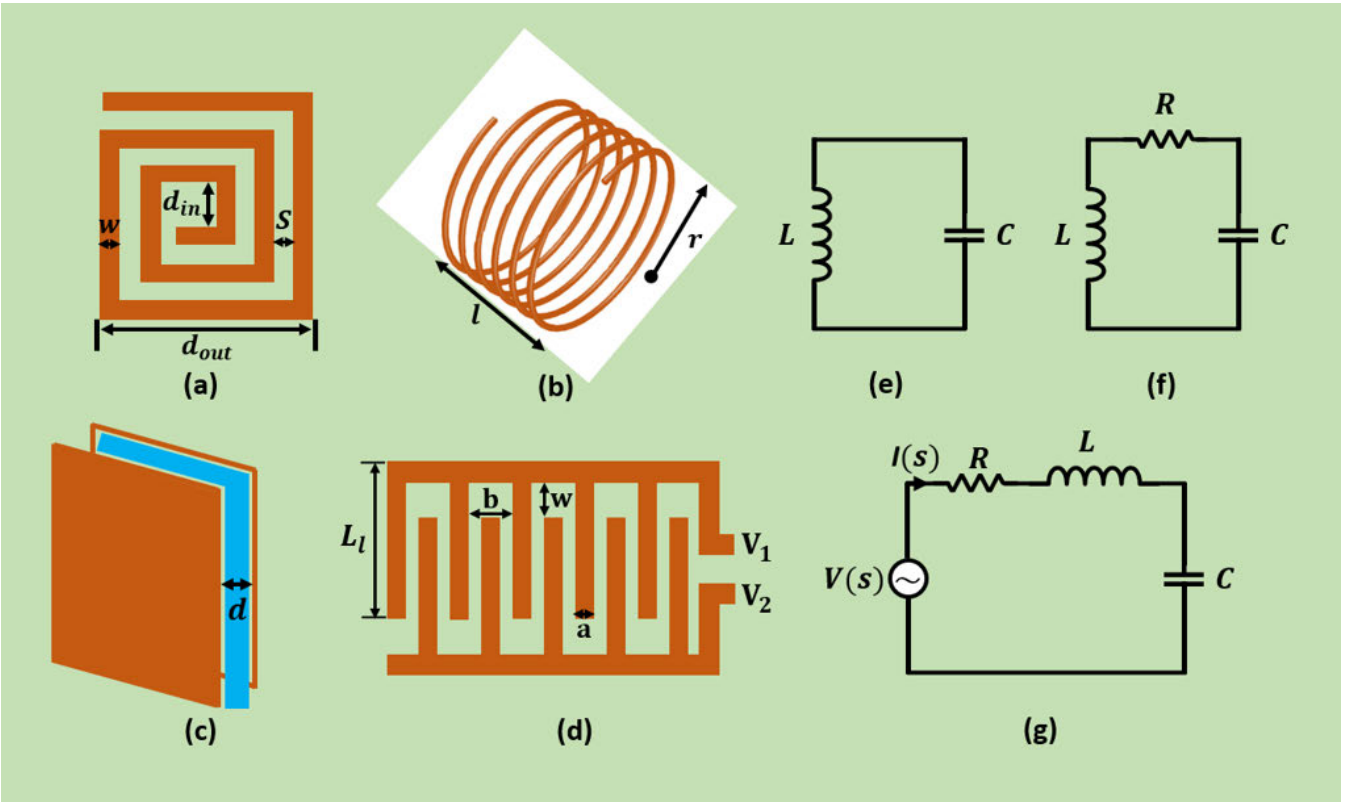

FIGURE 3. Schematic illustration of wireless *LC* resonant sensor components, (a) planar spiral inductor [48], (b) solenoid inductor, (c) parallel plate capacitor separated by distance *d*, (d) interdigitated capacitor [53], (e) *LC* resonant circuit, (f) *RLC* resonant circuit, (g) *RLC* resonant circuit with excitation source.

$\frac{R}{2L} < \frac{1}{\sqrt{LC}}$, respectively. When the equation (8) is underdamped condition, the roots become complex conjugate and can be written as:

$$s_{1,2} = -\frac{R}{2L} \pm j\sqrt{\frac{1}{LC} - \left(\frac{R}{2L}\right)^2} \tag{10}$$

where, $\frac{R}{2L} = \alpha$, damping constant $\omega_0 = \frac{1}{\sqrt{LC}}$, undamped natural resonant frequency $\omega_d = \sqrt{\omega_0^2 - \alpha^2}$, damped natural resonant frequency

The quantity ω_0 is the angular frequency of the oscillation when there is no resistive element is present in the circuit as Fig. 3. (e). On the other hand, the damped frequency ω_d is always less than the undamped natural resonant frequency due to the presence of resistive element in the circuit as shown in Fig. 3. (f).

However, the *RLC* resonant circuit exhibits both a natural and forced response when an excitation source is used. Depending on how much resistive element is present in the circuit, the *RLC* circuit's natural response can be underdamped, critically damped, or overdamped. Since resistive components are present in every practical *LC* circuit, the response of the circuit will always be transient in nature and die out after a short period of time for natural response. On the other hand, the forced response is determined by the circuit's excitation source. The source continuously maintains the response in the circuit after the transient has passed and the circuit has reached steady state, which is known as steady state response [54]. These resonant principles are utilized in frequency and time domain measurement technique to measure wireless *LC* resonant sensor, as discussed in section III.

Moreover, IA or VNA is often used to detect the resonant frequency of the sensors by monitoring the impedance of the readout coils or input return loss. These measuring isntruments are expensive and bulky, and are only suitable for laboratory measurements. A few compact electronics systems were reported by several research groups which require less complex circuitry and less power budget to interrogate the wireless *LC* resonant sensors [55], [56], [57], [58].

III. MEASUREMENT TECHNIQUES OF LC SENSORS

Two types of measurement techniques, namely frequency-domain and time domain are commonly used for wireless measurement of *LC* resonant sensors. This section covers analytical modeling, and corresponding numerical simulations of the *LC* sensors for both measurement domains, and highlighting their respective challenges.

A. FREQUENCY DOMAIN MEASUREMENT

The equivalent circuit of the magnetic coupling passive *LC* resonant sensor is depicted in Fig. 4. (a). The circuit can be

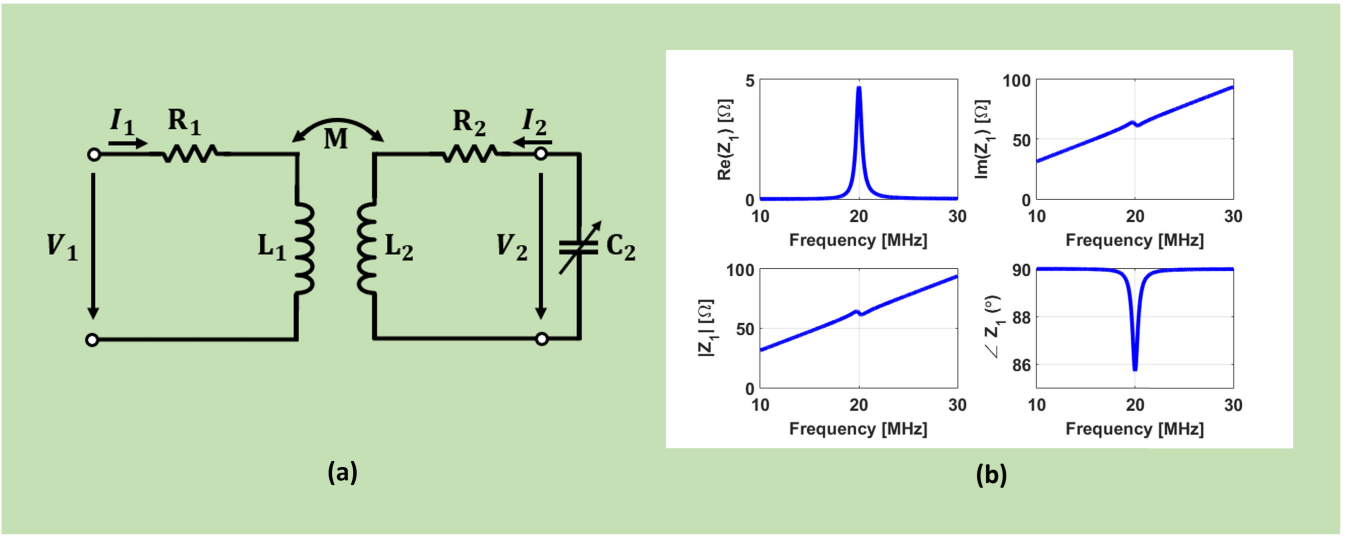

FIGURE 4. (a) Equivalent circuit of the inductively coupled *LC* sensor system [58], (b) numerical simulation of the equivalent impedance at the terminal of the readout coil with resonant frequency of the sensor $f_S = 20\text{MHz}$, $R_1 = 1\Omega$, $L_1 = 0.5\mu H$, $Q = 30$, and $k = 0.05$ [58].

expressed analytically using the impedance transformer equations for harmonic oscillations with complex frequency f, and the induced voltage in the primary coil L_1 and secondary coil L_2 can be written in the Laplace domain as follows [58]:

$$V_1 = R_1 I_1 + sL_1 I_1 + sMI_2 \tag{11}$$
$$V_2 = R_2 I_2 + sL_2 I_2 + sMI_1 \tag{12}$$

where V_1, V_2, I_1 and I_2 are the voltage and current of the primary and secondary sides of the inductive coupling coils, respectively. The equivalent series resistance of the primary and secondary coils is represented by the circuit elements R_1 and R_2, respectively. The parameter s is the complex frequency which can be written as $s = j\omega = j2\pi f$. The amount of inductive coupling between primary and secondary coil is measured by the mutual inductance M and can be written as:

$$M = k\sqrt{L_1 L_2} \tag{13}$$

where k is the geometry-dependent coupling coefficient of the mutual inductance M, which is dimensionless and ranges from 0 to ± 1. Maximum coupling occurs when $k = 1$, and no coupling occurs when $k = 0$. The sensing element of the *LC* circuit–capacitive sensor, C_2–is connected to the secondary coil L_2 of the inductive coupling, and the current flowing through the secondary part of the circuit can be written as:

$$I_2 = -sC_2 V_2 \tag{14}$$

The equivalent impedance Z_1 at the primary side or the readout coil can be derived by combining the equations (11), (12), and (14), i.e.,

$$Z_1 = \frac{V_1}{I_1} = R_1 + j2\pi f L_1 + \frac{(2\pi f)^2 M^2}{R_2 + j\left(2\pi f L_2 - \frac{1}{2\pi f C_2}\right)} \tag{15}$$

The resonance frequency f_S, and quality factor Q of the *LC* sensor can be written as follows:

$$f_S = \frac{1}{2\pi\sqrt{L_2 C_2}}, \quad Q = \frac{1}{R_2}\sqrt{\frac{L_2}{C_2}} \tag{16}$$

By substituting equation (16) in (15), the equivalent impedance Z_1 can be derived and separated between real and imaginary parts, i.e.,

$$Z_1 = R_1 + j2\pi f L_1 \left(1 + \frac{k^2 \left(\frac{f}{f_S}\right)^2}{1 + j\frac{f}{Qf_S} - \left(\frac{f}{f_S}\right)^2}\right) \tag{17}$$

$$R_e\{Z_1\} = R_1 + 2\pi f L_1 k^2 Q \frac{\frac{f}{f_S}}{1 + Q^2\left(\frac{f}{f_S} - \frac{f_S}{f}\right)^2} \tag{18}$$

$$I_m\{Z_1\} = 2\pi f L_1 \left(1 + k^2 Q^2 \frac{1 - \left(\frac{f}{f_S}\right)^2}{1 + Q^2\left(\frac{f}{f_S} - \frac{f_S}{f}\right)^2}\right) \tag{19}$$

The modulus of equivalent impedance $|Z_1|$, and phase angle $\angle Z_1$ can be written as follows:

$$|Z_1| = \sqrt{R_e^2\{Z_1\} + I_m^2\{Z_1\}} \tag{20}$$
$$\angle Z_1 = \tan^{-1}\frac{I_m\{Z_1\}}{R_e\{Z_1\}} \tag{21}$$

Fig. 4. (b) illustrates the numerically simulated frequency response of the equivalent impedance for the equations of (18), (19), (20), and (21) by incorporating the sensor parameters of $R_1 = 1\Omega$, $L_1 = 0.5\mu H$, $f_S = 20\text{MHz}$, $Q = 30$, and $k = 0.05$.

These derivations can be implemented in steady state or frequency domain measurement of wireless *LC* resonant sensors. Phase dip and dip meter are two measurement methods

that are frequently used in frequency domain analysis. The phase dip technique measures the equivalent impedance's phase angle, whereas the dip meter technique measures the maximum real part of the equivalent impedance Z_1.

1) PHASE DIP MEASUREMENT IN FREQUENCY DOMAIN

An IA or VNA is usually employed to determine the resonant frequency of the *LC* sensor by measuring the phase angle $\angle Z_1$ of the equivalent impedance in equation (21), and such measurement techniques have been reported in several publications [59], [60]. In phase dip measurement, the impedance phase minimum occurs at a frequency of $f_{\varphi,\min}$. The derivative of the equation (21) can be set to zero with respect to frequency f to obtain the analytical expression of the phase minimum, which can be expressed as [58]:

$$\frac{\partial \angle Z_1}{\partial f} = 0 \tag{22}$$

which yields $f_{\varphi,\min}$ as:

$$f_{\varphi,\min} \approx \left(1 + \frac{1}{4}k^2 + \frac{1}{8Q^2}\right) f_S \tag{23}$$

Equation (23) demonstrates that minimum phase of the equivalent impedance occurs at resonant frequency f_S not only depends on the quality factor Q but also depends on coupling coefficient k, which is a function of the geometrical dimension of two inductive coupling coils and their distances. Additionally, for an *LC* sensor with a sufficiently high-quality factor $Q \gg 1$ and relatively small coupling coefficient k the equation (23) leads to a phase dip at

$$f_{\phi,\min} \approx \left(1 + \frac{1}{4}k^2\right) f_S \tag{24}$$

which is still a function of the coupling coefficient k. Hence, measuring the resonant frequency f_S of the sensor by utilising the phase dip approach requires a large Q to achieve a sharper dip in the impedance phase, and at the same time, it also requires keeping the k value smaller [61]. Phase dip value can be calculated by the following expression [59]:

$$\Delta\varphi = \tan^{-1}\left(k^2 Q\right) \tag{25}$$

Measurement of *LC* sensors in the phase dip technique requires a fixed distance and specific orientation between the sensor and reader coil in order to keep k not too large or not too low for accurately tracking the resonant frequency of the sensor. A larger value of k exhibits a wider phase dip, shifting the resonant frequency f_S to higher frequencies as shown in Fig. 5. (a), while a smaller value of k produces a smaller magnitude of the phase dip, which is harder to track and lowers the SNR of the sensor measurement. Moreover, measuring a sensor at a fixed wireless distance is not practical in many real-time wireless applications which often require sensor or reader movements. Aside from the optimal value of the coupling coefficient k, phase dip measurement necessitates a sensor with a high-quality factor Q, as illustrated in Fig. 5. (b). The higher the sensor Q, the larger and sharper the phase dip magnitude, and the better the SNR of the readout signal. A high Q factor *LC* sensor could be achieved by increasing the size of the inductive coil of the sensors while keeping the internal resistance of the inductive trace as low as possible which is always a tradeoff between them as expressed in equation (16).

2) DIP METER MEASUREMENT IN FREQUENCY DOMAIN

Instead of measuring the phase dip of the equivalent impedance, a more robust measurement technique has been reported by several research groups which measures the real part of the maximum equivalent impedance [62], [63]. Numerical simulation of the real part of equivalent impedance in equation (18), as shown in Fig. 5. (c), shows that the coupling coefficient k only acts as an amplitude scaling factor and is independent of the sensor's resonance frequency f_S, and quality factor Q. The maximum frequency $f_{\max}$ and Full Width at Half Maximum (FWHM) can be obtained by following relations [58].

$$f_{\max} = \frac{2Q}{\sqrt{4Q^2 - 2}} f_S, \quad Q \approx \frac{f_S}{\Delta f_{\max}} \tag{26}$$

where $f_{\max}$ is the maximum frequency which can be obtained from the maximum of $R_e\{Z_1\}$ of equation (18), and $\Delta f_{\max}$ is the FWHM of $R_e\{Z_1\}$ at the origin of $f_{\max}$. Fig. 5. (d) shows the graphical representation of the $\Delta f_{\max}$ for a sensor of Q value of 105. For sufficiently large quality factor $Q \gg 1$, the $f_{\max}$ in equation (26) becomes the resonant frequency f_S of the sensor, $f_{\max} \approx f_S$, hence the sensor measurement is theoretically independent of the coupling coefficient k, and therefore distance independent measurement of the sensor. Moreover, one can obtain the value of the maximum impedance of the real part of equation (18) by setting $f = f_S$ which can be expressed as [42]:

$$Z_{\max} = R_e\,(Z_1)_{\max}\big|_{f=f_{\max}} = R_1 + 2\pi f_S L_1 k^2 Q \tag{27}$$

By comparing the effect of coupling coefficient k for both frequency domain measurement techniques, it is evident that the dip meter, or measuring the maximum real part of the equivalent impedance, provides theoretical distance-independent wireless measurement over the phase dip measurement technique as shown in Fig. 5. (a) and Fig. 5. (c), respectively.

B. TIME DOMAIN MEASUREMENT

In time domain or transient measurements, a pulse signal or modulated/ unmodulated signal is applied at the primary coil of the magnetic coupling for a short period of time, and damped decay response of the sensor is acquired at the primary or the readout coil of the sensor to determine the resonant frequency f_S and quality factor Q as shown in Fig. 6. (a) [38], [39]. The basic operating principle of the time domain measurement technique is depicted in Fig. 6. (b) and (c), respectively. In this measurement, sensor operation can be separated into two different phases of time: the excitation phase and the detection phase. The excitation phase provides an excitation signal to the sensors for a short

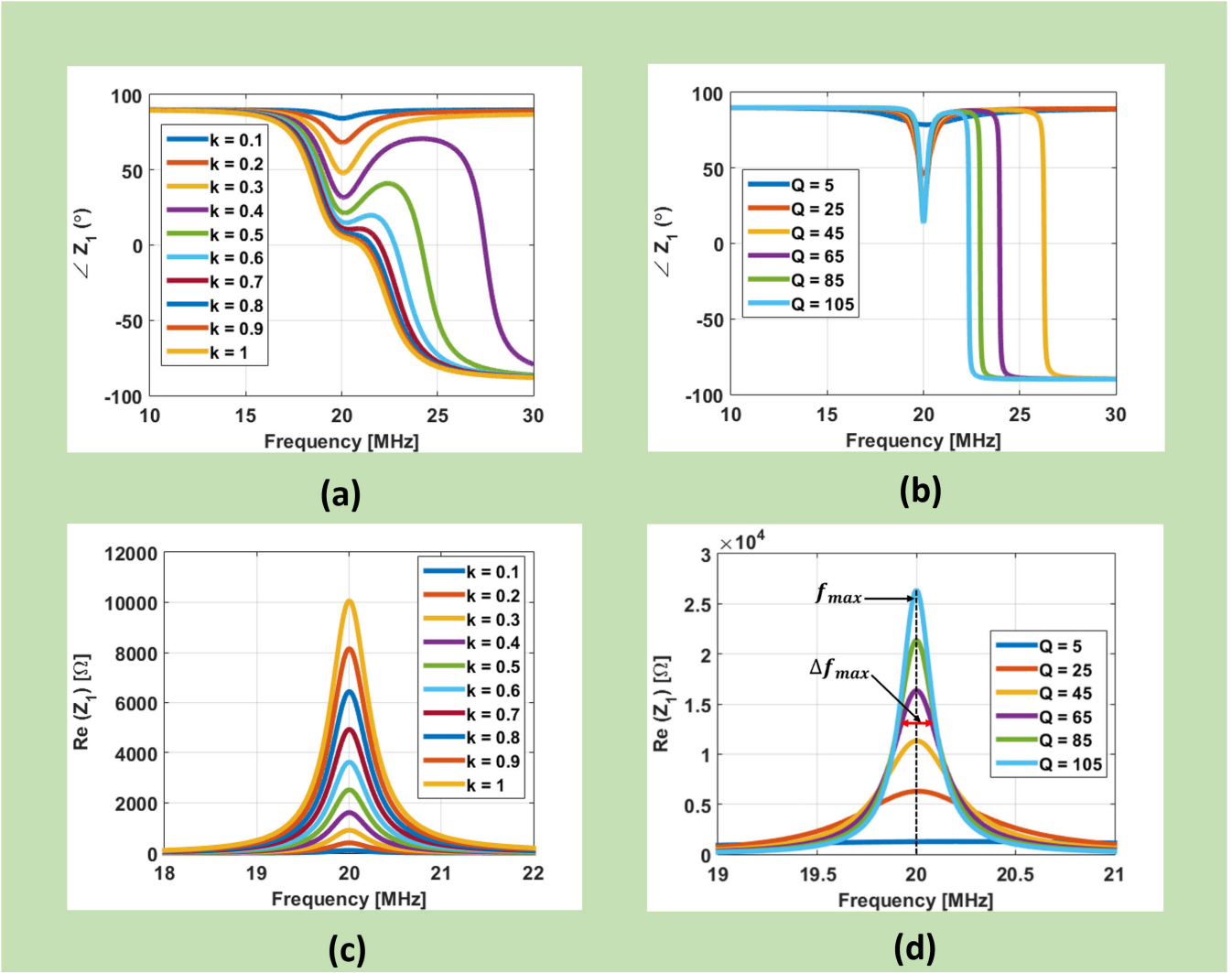

FIGURE 5. (a) Simulated equivalent impedance phase as a function of frequency for different values of coupling coefficient *k* [58], (b) the effect of different values of quality factor *Q* on the impedance phase, (c) maximum real part of the equivalent impedance as a function of frequency for different values of *k* [58], (d) the effect of different values of *Q* on the maximum real part of the equivalent impedance.

period of time. The following time phase is called the detection phase which acquires the damped decay response of the sensors. Fischer et al. reported time domain measurement of a resonant sensor where the sensor's damped decay response f_d is measured at the secondary coil, which is an integral part of the sensor [26]. However, measuring the sensor response at the primary coil allows for complete isolation of the sensor from the reader, which is a more practical case for wireless resonant sensor measurement.

The analytical modeling of time domain measurement has considered sensors detection phase as shown in Fig. 6. (c), since the sensor excitation phase only provides the excitation signal to the sensor, which does not have an active role during the detection phase. The impedance of primary and secondary coils can be represented as $Z_1 = R_1 + sL_1$ and $Z_2 = R_2 + sL_2$, respectively, where s is the complex frequency in the Laplace domain. During the detection phase, energy storage elements in an inductively coupled sensor circuit are no longer relaxed. For analytical analysis, one needs to consider the effects of initial conditions on the sensor readout signal, and for all the initial conditions $t > 0$, which only affects the starting amplitude of the readout signal and does not alter the complex frequency of the sensor [64]. Hence, the single initial condition denoted by V_{C20} can be considered an effective initial condition, which is the voltage across the capacitive sensor C_2 at $t = 0$, neglecting other initial conditions as shown in Fig. 6. (d). The equivalent circuit for time domain measurement during the detection phase can be analysed in the Laplace domain and the readout signal can be expressed as follows [64]:

$$V_1(s) = k\sqrt{\frac{L_1}{L_2}}V_{C20}\frac{s}{s^2 + s\frac{R_2}{L_2} + \frac{1}{L_2C_2}} \tag{28}$$

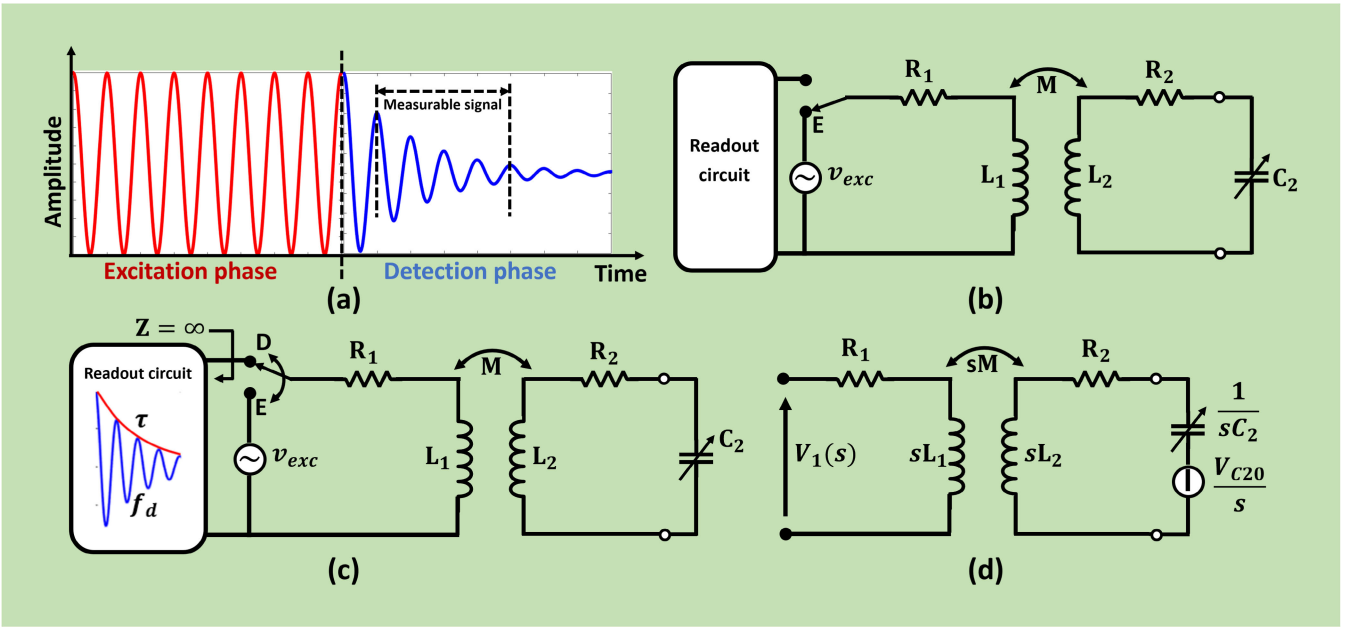

FIGURE 6. Block diagram of the time domain measurement technique, (a) excitation and detection signal representation of the time domain measurement, (b) block diagram of the excitation phase of the *LC* sensors [64], (c) block diagram of the detection phase of the *LC* sensors [64], (d) equivalent circuit of the *LC* sensors during the detection phase [64].

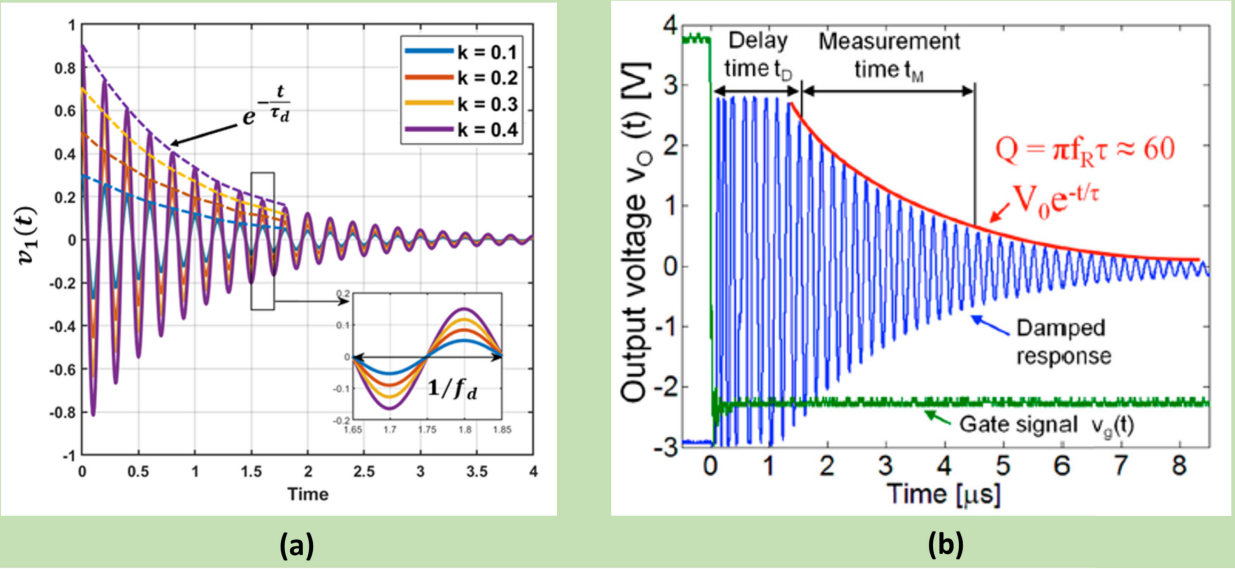

FIGURE 7. (a) Simulation on the effect of different values of coupling coefficient *k* on the amplitude and the length of the readout signal [64], (b) measured output voltage versus time during the detection phase of the sensors. The delay time t_D is used to avoid the initial glitch of the damped signal, and the measurement time t_M represents the sensor measurement time. The envelope of the damped decay signal approximates the quality factor of the sensor [38].

The corresponding expression of the readout signal $V_1(s)$ can be calculated in the time domain

$$v_1(t) = kabV_{C20}e^{-\frac{t}{\tau_d}} \cos\left[2\pi f_d t - \tan^{-1}\left(\frac{1}{2\pi f_d \tau_d}\right)\right] \tag{29}$$

where $a = \sqrt{\frac{L_1}{L_2}}$, and $b = \sqrt{\frac{4Q^2}{4Q^2-1}}$

The signal $v_1(t)$ is a damped decay sinusoidal with a damped frequency f_d and decay time τ_d which are connected to the resonant frequency f_S and quality factor Q of the sensor, and they can be expressed as follows:

$$f_d = \sqrt{1 + \frac{1}{4Q^2}} f_S \quad , \quad \tau_d = \frac{Q}{\pi f_S} \tag{30}$$

where for a sufficiently larger Q, the damped frequency f_d becomes the resonant frequency f_S of the sensor as $f_d \approx f_S$, with a relative deviation $|f_d - f_S|/f_S < 50$ for $Q > 50$. It can be observed from equation (29) that the coupling coefficient k only acts as an amplitude scaling factor of the damped sinusoidal signal $v_1(t)$, where the damped frequency f_d and decay time τ_d are unaffected by coupling coefficient k. Therefore, the resonant frequency f_S of the wireless LC sensor in time domain measurement is theoretically independent of the coupling coefficient k. Fig. 7. (a) shows the readout signal $v_1(t)$ for different values of k, which only affect the amplitude of the signal without altering the damped frequency f_d.

IV. MEASUREMENT CHALLENGES OF LC SENSORS

Analytical modeling of the wireless LC resonant sensors for two measurement techniques, dip meter in the frequency domain and transient or time domain measurement, showed in section (III) that the resonant frequency f_S and quality factor Q of the sensor are theoretically independent of the coupling coefficient k, resulting in a distance-independent wireless measurement of the sensors. Nevertheless, when these two measurement techniques are utilised in real electronics equipment or circuits; unavoidable parasitic capacitance C_P appears in parallel to the readout coil, which comprises all the contributions from the parasitic capacitance present in the primary coil L_1, the capacitance of the connections, and the input capacitance of the electronic interface [64], [65]. The presence of finite parasitic capacitance C_P significantly degrades the measurement accuracy of the resonant frequency f_S and the quality factor Q of the sensors. The following sections discuss the effect of parasitic capacitance C_P for dip meter in frequency domain and time domain measurement as depicted in Fig. 8. (a) and Fig. 8. (b).

A. EFFECTS OF PARASITIC CAPACITANCE IN DIP METER MEASUREMENT

Limitations associated with measuring the maximum real part of the equivalent impedance in dip meter measurement in frequency domain are due to the presence of unavoidable finite parasitic capacitance C_P, which appears in parallel to the readout coil of the LC sensor as shown in Fig. 8. (a) [65]. When the presence of parasitic capacitance is not negligible, the real part of the equivalent impedance Z_{1P} becomes [65]:

$$R_e\{Z_{1P}\} = R_e\left\{\frac{\left(m + \frac{4\pi^2 f^2 k^2 L_1 L_2}{R_2 + j2\pi f L_2 + \frac{1}{j2\pi f C_P}}\right)\frac{1}{j2\pi f C_P}}{m + \frac{4\pi^2 f^2 k^2 L_1 L_2}{R_2 + j2\pi f L_2 + \frac{1}{j2\pi f C_P}} + \frac{1}{j2\pi f C_P}}\right\} \quad (31)$$

where $m = R_1 + j2\pi f L_1$. Equation (31) shows that the coupling coefficient k not only acts as an amplitude scaling factor but without knowing the value of k priori, it is not possible to extract the resonant frequency f_S, and quality factor Q of the sensor independently. The numerical analysis illustrates that there are two maxima of the real part of equivalent impedance Z_{1P} are influenced by the coupling coefficient k–when parasitic capacitance C_P is fixed and coupling coefficient k is variable in Fig. 9. (a); and parasitic capacitance C_P is variable while coupling coefficient k is fixed in Fig. 9. (b)–corresponds to a primary resonance near $f_S = 1/\left(2\pi\sqrt{L_2 C_2}\right)$ and a secondary resonance near $f_P = 1/\left(2\pi\sqrt{L_1 C_P}\right)$, respectively [65], [66]. The numerical simulation and the measurement result exhibit that when C_P is non-negligible, the maximum real of the equivalent impedance is not distance independent as shown in Fig. 9. (a) and (b), and Fig. 10. (a) indicating no compensation, respectively.

B. EFFECTS OF PARASITIC CAPACITANCE IN TIME DOMAIN MEASUREMENT

The analytical modeling of time domain measurement discussed in section (III) B showed that the damped frequency f_d of the sensor is theoretically independent of the wireless interrogation distance. However, the analytical expression of time domain measurement by considering the parasitic capacitance was derived in the Laplace domain, and it could be written as [64]:

$$V_{1P}(s) = k\sqrt{\frac{L_1}{L_2}}\frac{sV_{C20}C_2L_2}{s^4C_2C_PL_1L_2\left(1-k^2\right) + s^3x + s^2y + sz + 1} \quad (32)$$

where

$$x = C_2C_P\left(L_1R_2 + L_2R_1\right),$$
$$y = C_2L_2 + C_PL_1 + C_2C_PR_1R_2,$$
$$z = C_2R_2 + C_PR_1$$

It can be seen from equation (32) that the coupling coefficient k is not only acting as an amplitude scaling factor but is also connected to the coefficient of the fourth-order polynomial at the denominator. Since the fourth order polynomial can be decomposed into two pairs of complex conjugate roots and the S^4 term is connected to the coupling coefficient in the form of $\left(1-k^2\right)$, it is expected that the complex frequencies (for $s = j\omega$) will depend on k. The inverse Laplace transform of the equation (32) shows that the output voltage signal is composed of the sum of two damped sinusoids and can be expressed as follows:

$$v_{1C_p}(t) = A_1e^{-\frac{t}{\tau_{d1}}}\cos\left(\omega_{d1}t - \theta_1\right) + A_2e^{-\frac{t}{\tau_{d2}}}\cos\left(\omega_{d2}t - \theta_2\right) \quad (33)$$

where A_1 and A_2 are the amplitude coefficients, θ_1 and θ_2 are the phase angle of the readout signal, which depends on the parameters of the circuits and the initial conditions. Damped frequencies ω_{d1} and ω_{d2}, and the decay times τ_{d1} and τ_{d2} can be obtained from two pairs of complex conjugate poles by setting the denominator of the equation (32) equal to zero. The values of the two pairs of complex conjugate poles can be further derived and seen that the decay time τ_{d2} is larger than τ_{d1} and, the resulting damped sinusoid ω_{d1} falls faster

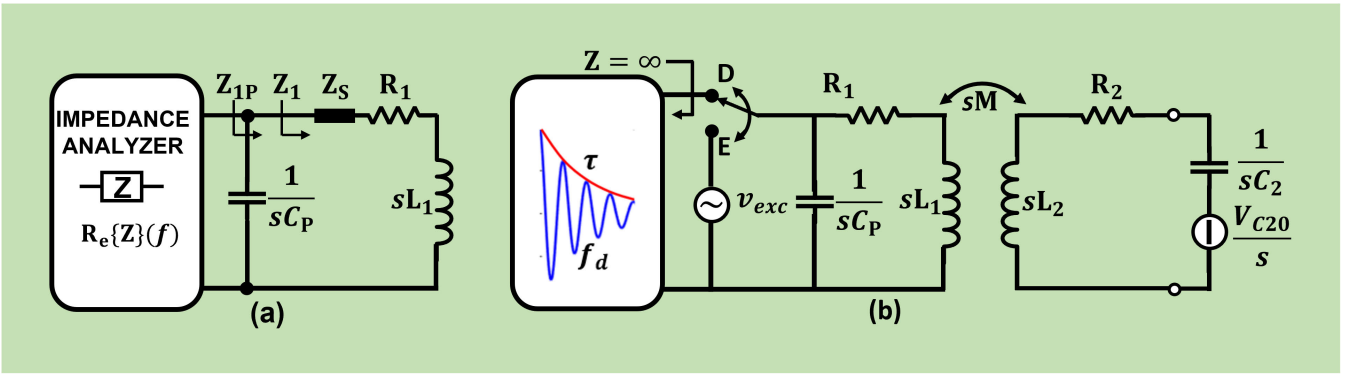

FIGURE 8. (a) Block diagram of the frequency domain measurement of wireless *LC* sensor by an impedance analyser with the presence of parasitic capacitance C_P [64], (b) block diagram of the time domain measurement of the *LC* sensor and its equivalent circuit in Laplace domain under the presence of parasitic capacitance C_P in parallel to the readout signal [64].

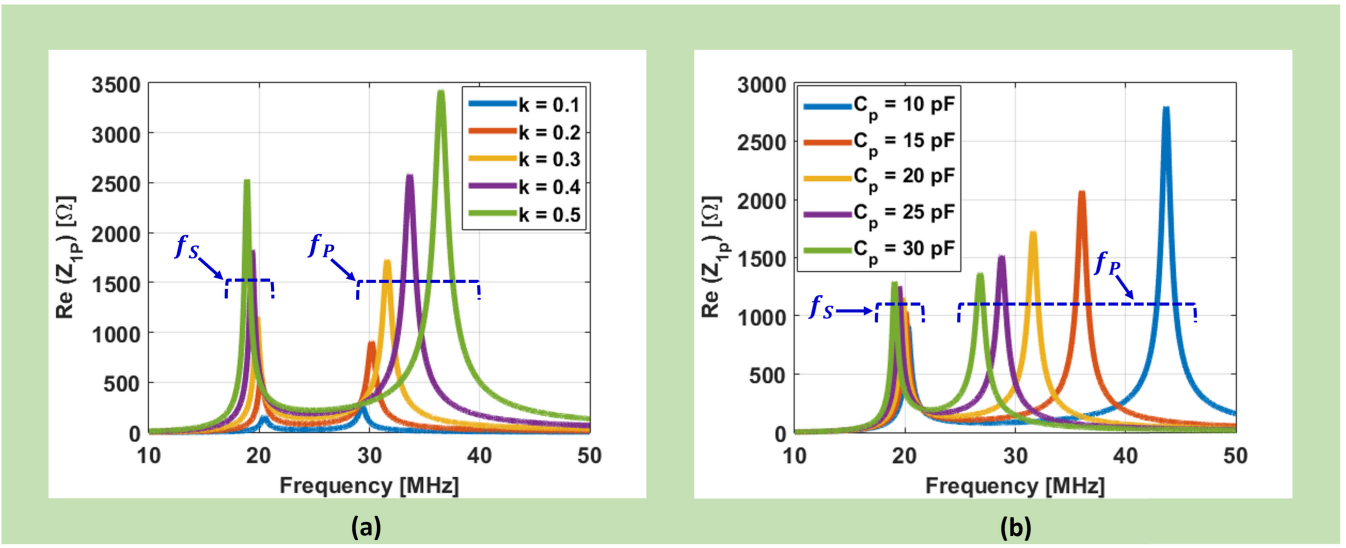

FIGURE 9. (a) Numerical simulation of the real part of equivalent impedance under the presence of parasitic capacitance C_P with increasing values of coupling coefficient *k* [66], (b) simulation of the real part with varying parasitic capacitance C_P [66].

than that ω_{d2}. Since both ω_{d1} and ω_{d2} are dependent on the coupling coefficient k, the effect of parasitic capacitance C_P ceases the distance independent measurement of the *LC* sensor. Therefore, the effect of parasitic capacitance is non-negligible for distance independent measurement of wireless *LC* sensors in both frequency and time domain, and the presence of parasitic capacitance C_P contributes to an inaccurate measurement of the resonant frequency f_S, and quality factor Q of the sensors.

V. PARASITIC CAPACITANCE COMPENSATION TECHNIQUE

The presence of parasitic capacitance in parallel to the readout coil in both measurement techniques–dip meter in frequency domain and time domain–results in distance dependent measurement of the wireless *LC* resonant sensors. For dip meter measurement, the maximum real part of the equivalent impedance is theoretically independent of the distance, hence k, when parasitic capacitance C_P is not present in the readout coil as shown in numerical simulation in Fig. 5. (C). In contrast, when the parasitic capacitance C_P is non-negligible as shown in Fig. 11. (C), the measurement of the maximum real part of equivalent impedance becomes wireless distance dependent measurement of the sensor, hence k dependent, as shown by numerical simulation in Fig. 9. (a), (b), and by the experimental result in Fig. 10. (a) indicating no compensation.

On the other hand, for time domain measurement, the damped decay response of the sensor is independent of the wireless distance and hence k, when the parasitic capacitance is not present at the readout coil as shown in numerical simulation Fig. 7. (a). However, the parasitic capacitance C_P appears during the detection phase of the sensor as shown in Fig. 11. (b). The experimental result shown in Fig. 10. (b) indicating no compensation demonstrates the distance dependent measurement of the sensor when C_P is non-negligible.

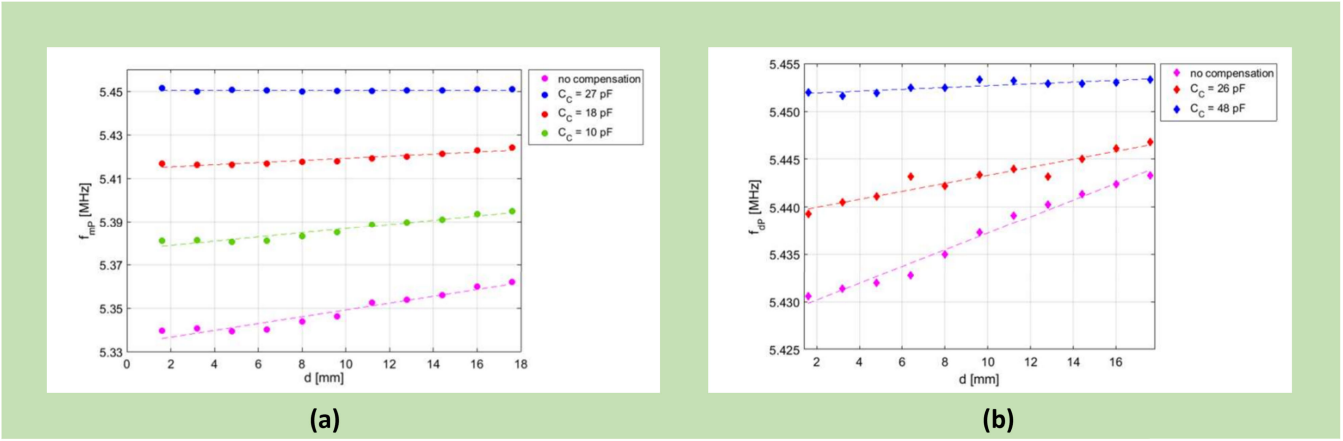

FIGURE 10. (a) Measurement of the maximum real part of $R_e\{Z_1\}$ for different wireless interrogation distance without using capacitance compensation circuit indicating as no compensation and with capacitance compensation circuit in parallel to the readout coil as indicated C_C [64], (b) measurement of the damped decay response for different wireless distances without capacitance compensation circuit indicating no compensation and with a capacitance compensation circuit indicating C_C [64].

Therefore, to overcome the effects of parasitic capacitance, a compensation circuit has been proposed by Demori et al. which can be connected to the sensor readout coil to eliminate the presence of unavoidable parasitic capacitance C_P for both frequency and time domain measurement and can significantly improve the accuracy of distance independent measurement of the sensors [64], [65]. The proposed circuit acts as a negative impedance converter which provides an equivalent impedance, where negative capacitance can be tuned to compensate and possibly cancel the parasitic capacitance C_P [65], [66]. The Fig. 11. (a) shows the block diagram of the parasitic capacitance compensation circuit which is an operational amplifier with a positive feedback, and will be connected in parallel to the readout coil L_1. The induced voltage V_1 across the readout coil L_1 is then fed to the capacitance C_A and the current flowing through the capacitance C_A can be written as follows [65]:

$$I_1 = \frac{V_1 - AV_1}{\frac{1}{sC_A}} = -\frac{R_F}{R_G} sC_A V_1 \tag{34}$$

where $A = \left(1 + \frac{R_F}{R_G}\right)$ is the non-inverting gain of the operational amplifier. Therefore, the equivalent input impedance Z_{Eq} of the amplifier can be written from equation (34) as follows:

$$Z_{Eq} = \frac{V_1}{I_1} = -\frac{R_G}{R_F sC_A} = -\frac{R_G}{j\omega C_A R_F} = \frac{1}{j\omega\,(-C_c)} \tag{35}$$

where $-C_c = -C_A \frac{R_F}{R_G}$, indicating that the circuit simulates an effective negative capacitance. From equation (35), if the gain of the amplifier is made adjustable, i.e. making the feedback resistor R_F as a variable resistance, $-C_c$ can be tuned to compensate and possibly cancel the parasitic capacitance C_P [65], [66]. The cancellation of C_P will lead the equation (31) to become equation (18) as $R_e\{Z_{1P}\} = R_e\{Z_1\}$ and equation (32) become in equation (28) as $V_{1P}(S) = V_1(S)$. Therefore, cancelation of the C_P results in distance independent measurement of LC resonant sensor in both measurement techniques: frequency domain in dip meter and time domain.

Fig. 10. (a) shows the measurement of the maximum real part of equivalent impedance for different wireless distances after introducing the parasitic compensation circuits as indicating C_C [64]. It can be observed that the resonant frequency f_S of the LC sensor which is the maximum real part of the equivalent impedance is identical throughout the variation of wireless interrogation distances when the compensation capacitance $C_C = 27$ pF, resulting in distance independent measurements. Similarly, the capacitance compensation circuit is employed to measure the damped frequency f_d of the LC sensors for different wireless distances in time domain measurement, as shown in Fig. 10. (b) indicating C_C [64]. It can be seen that without compensation circuit, the measurement of damped frequency f_d in time domain exhibits inaccuracies.

VI. DISCUSSION

Wireless passive LC resonant sensors have been widely investigated in various fields of applications due to their numerous benefits. These benefit include passive operation, which eliminates the need for an active power supply. Their sensing elements, such as inductors and capacitors, are relatively easy to fabricate. These sensors have a robust sensing operating principle based on resonance and are suitable for handheld sensor applications. Despite all these advantages, the need for complex or bulky readout systems remains a bottleneck for adoption of handheld wireless sensor measurements. For widespread application of LC sensors, it is of utmost importance to design a compact, simple, low power and cost-effective reader system, which is unavailable in current practice.

One of the most desirable features of the wireless LC sensor is to have an increased wireless interrogation distance. Since the LC sensor is formed with a combination of

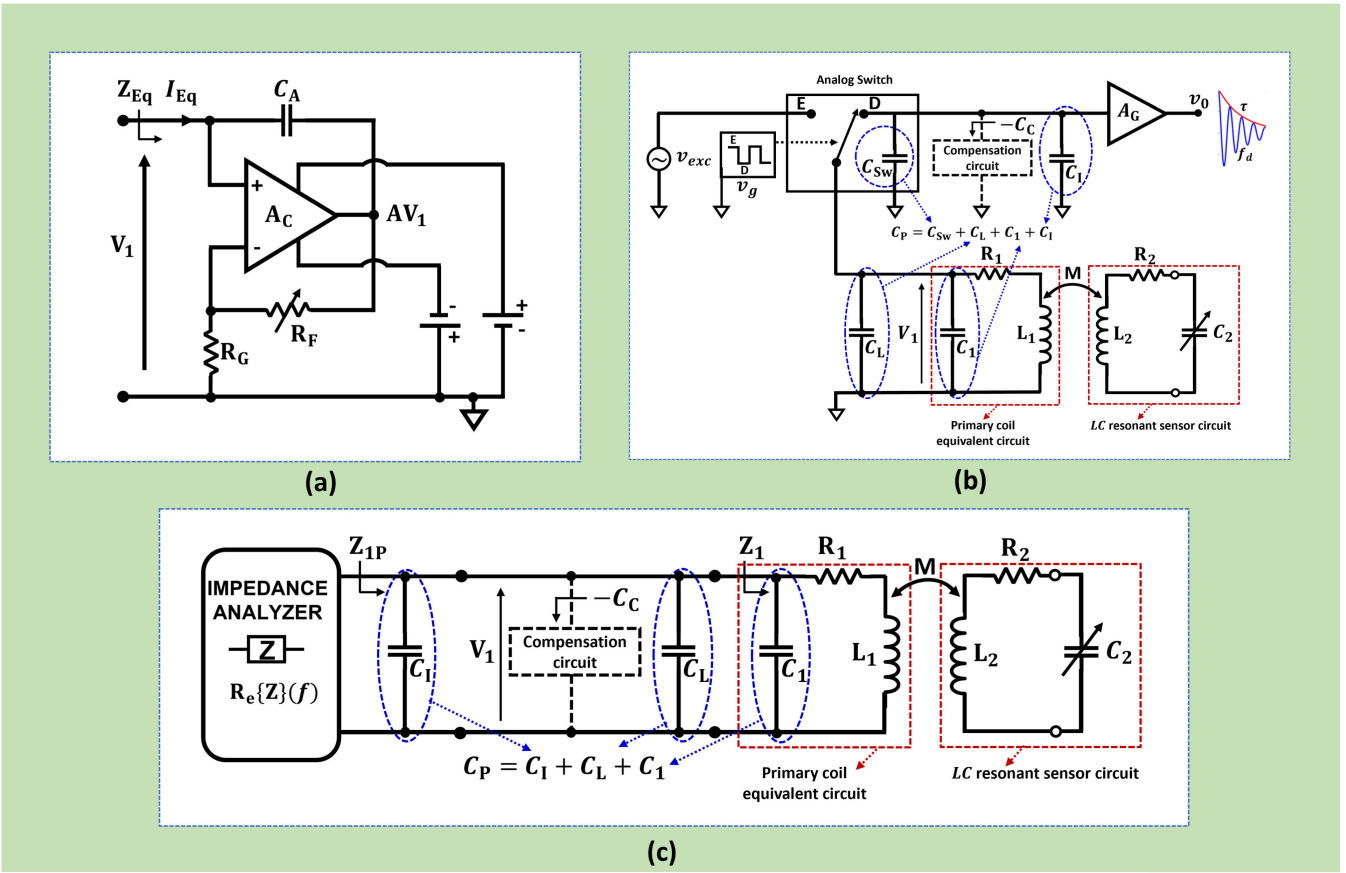

FIGURE 11. (a) Block diagram of the parasitic capacitance compensation circuit [66], (b) the effect of parasitic capacitance C_P appears in parallel to the readout coil of the *LC* sensor during the detection phase of the time domain measurement. The parasitic capacitance C_P is the sum of all the parasitic capacitance contributions such as capacitance of the analog switch C_{sw}, capacitance of the connection C_L, capacitance between traces of the primary coil C_1, and input capacitance of the readout amplifier C_I which appears in parallel to the readout coil. Parasitic capacitance compensation circuit in Fig. 11. (a) is connected in parallel to the readout coil to cancel the effect of C_P [64], (c) the effect of C_P in frequency domain dip meter measurement. Different parasitic capacitance contributes to C_P in parallel to the readout coil namely impedance analyser input capacitance C_I, capacitance of the connection C_L, and capacitance between traces of primary coil C_1. The compensation circuit in Fig. 11. (a) is employed in parallel to the readout coil to cancel the effect of C_P [64].

an inductive coil with a capacitor, increasing the size of a inductive coil can effectively increase the magnetic coupling between the sensor and readout coil, resulting in an increased wireless distance. However, increasing the size of a inductive coil that connects with the capacitive sensing element, increases the overall footprint of the *LC* sensor, which makes it difficult to deliver and place the sensor in many applications such as biomedical implantation. The advancement of micro-electromechanical systems (MEMS) and flexible printing technologies have enabled miniaturisation of sensor footprints but reducing the coil size of the sensors has a significant effect on the wireless interrogation distance and quality factor Q of the sensor, which essentially reduce the measurement distance and SNR of the readout signal.

In 2008, Chen et al., proposed parylene based micromachined wireless *LC* pressure sensors with a footprint of $4 \times 1\ \text{mm}^2$, an operating frequency of 150 MHz, and a quality factor of 5 that achieved the wireless distance of 2 mm [67]. Xue et al., developed an *LC* pressure sensors made of SU-8 and Gold with a footprint of $3.23 \times 1.52 \times 0.2\ \text{mm}^3$, achieved a wireless distance of 6 mm, with operating frequency of 250 MHz, and a quality factor of 21.3 [68]. Later on Chen et al, developed an improved version of pressure sensor with parylene C having a quality factor of 30 which covers the wireless distance more than 20 mm with operating frequency of approximately 350 MHz, evidencing the increased wireless distance with improved quality factor Q of the sensor [52].

In order to increase the inductance value of the sensor coil, a multilayer inductor can be used as reported in [60] and [61]. However, at high-frequency sensor operation, the parasitic capacitance between the inductive coil traces comes into play and needs careful handling. Moreover, the value of the inductive coil of the sensor can be increased by introducing a magnetic material such as a ferrite core with the inductive coil to obtain a stronger coupling between the wireless interrogating coils. Harpster et al. proposed a humidity sensor based on polymide as sensitive capacitor and solenoid

TABLE 1. Comparison of relative deviation of sensor operating frequency $(f - f_S)/f_S$ across wireless distance ranges in different measurement techniques.

L_2	C_2	R_2	f_S	Q	Considered distance, d	$(f - f_S)/f_S$ (%)	Comments	Reference
3.5μH	5pF	-	38MH_Z	-	$0-62$ mm	4.71	Phase dip measurement technique in frequency domain, $(f - f_S)/f_S(\%)$ derived from Fig.8 in [69].	[69]
8.35μH	4.37pF	9.35Ω	26.3MH_Z	-	$0-60$ mm	10.8	Phase dip measurement technique in frequency domain, $(f - f_S)/f_S(\%)$ derived from Fig.4 in [70].	[70]
11.4μH	15pF	-	12.2MH_Z	-	$0-6$ mm	0.78	Gate dip measurement technique in frequency domain, $(f - f_S)/f_S(\%)$ derived from Fig.5 in [71].	[71]
1.92μH	0.397pF	-	178MH_Z	6.5	$0-18$ mm (vertical)	6.74	Phase dip measurement technique in frequency domain, $(f - f_S)/f_S(\%)$ derived from Fig.8. (a) in [72].	[72]
1.92μH	0.397pF	-	178MH_Z	6.5	$0-14$ mm (horizontal)	7.86	Phase dip measurement technique in frequency domain, $(f - f_S)/f_S(\%)$ derived from Fig.8. (a) in [72].	[72]
8.5μH	104.7pF	3.2Ω	5.3MH_Z	89	$0-24$ mm	$0.02 <$	Dip meter measurement technique in frequency domain with parasitic capacitance compensation circuit, $(f - f_S)/f_S(\%)$ derived from Fig. 6 in [65].	[65]
8.51μH	100pF	3.2Ω	5.45MH_Z	91	$1.6-17.6$ mm	$0.02 <$	Dip meter measurement technique in frequency domain with parasitic capacitance compensation circuit, $(f - f_S)/f_S(\%)$ derived from Fig. 19 in [64].	[64]
8.5μH	99pF	3.2Ω	5.48MH_Z	91.5	$1.6-14.4$ mm	$0.02 <$	Dip meter measurement technique in frequency domain with parasitic capacitance compensation circuit, $(f - f_S)/f_S(\%)$ derived from Fig. 4. (a) in [66].	[66]
8.51μH	100pF	3.2Ω	5.45MH_Z	91	$1-17.6$ mm	$0.03 <$	Time domain measurement with parasitic capacitance compensation circuit, $(f - f_S)/f_S(\%)$ derived from Fig. 23 in [64].	[64]

coil wound around a ferrite substrate to improve the wireless distance upto 20 mm [73]. However, integrating magnetic material further increases the size of the coil, and weight of the sensors.

A high-quality factor Q is always desirable for the wireless operation of the LC sensors which essentially increases the wireless interrogation distance between the sensor and reader as well as improves the accuracy of sensors measurements. The quality factor Q of the LC sensor can be improved by tackling the losses that are present in the sensors. These losses include copper conduction losses in inductive coil, dielectric losses in dielectric material of the sensing element–capacitor–, skin effects, and radiation losses [74], [75]. The copper conduction losses are mainly the resistive loss which is always present for both low and high frequency sensor operation and can be compensated by selecting high conductive coil materials, resulting a lower equivalent series resistance of the coil. For high frequency applications, skin effects appear on coil surfaces which contributes to high frequency losses of the LC sensor. Such high frequency losses can be reduced by using litz wire to design inductive coil [76], [77]. The dielectric loss can be tackled by selecting low-loss dielectric material for the sensing element and the radiation loss can be tackled by shielding the sensor during high frequency operation.

Furthermore, it has been shown in section (III) that for dip meter and phase dip sensor measurement, a high Q sensors provides a sharper peak in both measurements. The numerical simulation in Fig. 5. (d) shows that measuring the maximum of the real part of equivalent impedance for a sensor with a quality factor $Q = 105$ is 2.3 times higher than measuring the maximum of the real part of equivalent impedance for a sensor with a $Q = 25$, resulting in a higher value of the equivalent impedance and, thus, an improved SNR for the readout signal. For time domain measurement, as reported in equation (30), the damped decay frequency becomes the resonant frequency of the sensor when high Q of a sensors is ensured. The damped decay signal for $k = 0.4$ indicates the higher Q value than the $k = 0.1$, as shown in Fig. 7. (a), where the Q of a sensor is extracted from the exponential envelope of the decay signal as e^{-t/τ_d}. Furthermore, Fig. 7. (a) shows that the amplitude and length of the decay signal increase with high Q value of the sensor. Therefore, measurability of sensors readout greatly improves for higher value of Q in both frequency and time domain measurement, by improving the SNR of the readout signal.

The coupling coefficient k between the two inductive coils L_1 and L_2 has also a significant effect on the sensor readout signal, since k depends on the geometrical parameters of the coils such as their distances, and relative orientation. Hence, many wireless LC resonant sensors are measured by keeping such geometrical parameters fixed and constant. However, in many practical wireless LC sensor applications, keeping the distance and alignment between the sensors coils fixed and constant is impractical, and requires k independent measurement of the sensors. This review has shown that the measurement of the real part of the equivalent impedance of the readout coil in frequency domain, and measuring the voltage of the readout coil in the time domain are theoretically independent of the coupling coefficient k, hence not affected by the distance between the sensor and the reader circuit. But the presence of parasitic capacitance, which appears in parallel with the readout coil of the sensor for both frequency and time domain measurement eliminates the integrity of k in a distance-independent wireless measurement of the sensors. To resolve the k dependence in these measurements, a compensation circuit is required to cancel the unavoidable parasitic capacitance. The Table 1 shows the comparison of relative deviation of the resonant frequency across wireless distance ranges in different measurement techniques with and without parasitic capacitance compensation circuit. It can be observed that the relative deviation of the resonant frequency significantly reduced to 0.02% for the measurement where a compensation circuit has been employed.

VII. CONCLUSION

The fundamental operating principles of the wireless passive LC sensors, and their measurement techniques, such as time and frequency domain, have been reviewed, as well as how these two methods can precisely measure the resonance frequency of the sensor. Phase dip measurement in the frequency domain has been applied in many applications, but accurate sensor measurement using the phase dip technique requires a fixed wireless distance because phase dip measurement is highly dependent on the coupling coefficient k, and thus not suitable for wireless distance independent sensor measurement. The dip meter measurement in the frequency domain and the damped decay response in the time domain measurement, on the other hand, are theoretically independent of the k, resulting in distance independent wireless measurement of the sensor. However, both measurement techniques suffer from unavoidable parasitic capacitance which appears in parallel to the sensor's readout coil, resulting in a distance dependent wireless sensor measurement. Such undesired dependency due to the presence of parasitic capacitance can be reduced significantly or completely eliminated when a parasitic compensation circuit is employed in parallel to the readout coil. This information will be of great value for future development of LC sensors that require accurate wireless readout.

REFERENCES

[1] R. S. Mackay and B. Jacobson, "Endoradiosonde," *Nature*, vol. 179, pp. 1239–1240, Jun. 1957, doi: 10.1038/1791239a0.

[2] C. C. Collins, "Miniature passive pressure transensor for implanting in the eye," *IEEE Trans. Biomed. Eng.*, vol. BME-14, no. 2, pp. 74–83, Apr. 1967, doi: 10.1109/TBME.1967.4502474.

[3] S. E. Woodard, C. Wang, and B. D. Taylor, "Wireless temperature sensing using temperature-sensitive dielectrics within responding electric fields of open-circuit sensors having no electrical connections," *Meas. Sci. Technol.*, vol. 21, no. 7, May 2010, Art. no. 075201, doi: 10.1088/0957-0233/21/7/075201.

[4] C. Zhang, L.-F. Wang, J.-Q. Huang, and Q.-A. Huang, "An LC-type passive wireless humidity sensor system with portable telemetry unit," *J. Microelectromech. Syst.*, vol. 24, no. 3, pp. 575–581, Jun. 2015, doi: 10.1109/JMEMS.2014.2333747.

[5] B. E. Horton, S. Schweitzer, A. J. DeRouin, and K. G. Ong, "A varactor-based, inductively coupled wireless pH sensor," *IEEE Sensors J.*, vol. 11, no. 4, pp. 1061–1066, Apr. 2011, doi: 10.1109/JSEN.2010.2062503.

[6] S. H. Song, J. H. Park, G. Chitnis, R. A. Siegel, and B. Ziaie, "A wireless chemical sensor featuring iron oxide nanoparticle-embedded hydrogels," *Sens. Actuators B, Chem.*, vol. 193, pp. 925–930, Mar. 2014, doi: 10.1016/J.SNB.2013.12.012.

[7] M. Farooq, T. Iqbal, P. Vazquez, N. Farid, S. Thampi, W. Wijns, and A. Shahzad, "Thin-film flexible wireless pressure sensor for continuous pressure monitoring in medical applications," *Sensors*, vol. 20, no. 22, p. 6653, Nov. 2020, doi: 10.3390/S20226653.

[8] M. Farooq, B. Amin, M. J. Kraśny, A. Elahi, M. R. U. Rehman, W. Wijns, and A. Shahzad, "An ex vivo study of wireless linkage distance between implantable LC resonance sensor and external readout coil," *Sensors*, vol. 22, no. 21, p. 8402, Nov. 2022, doi: 10.3390/S22218402.

[9] M. Ferrari, M. Baù, M. Masud, and V. Ferrari, "A time-gated contactless interrogation system for frequency and quality factor tracking in QCR to investigate on liquid solution microdroplets," *Proc. Eng.*, vol. 168, pp. 704–707, Jan. 2016, doi: 10.1016/J.PROENG.2016.11.252.

[10] M. Fonseca, M. Allen, J. Kroh, and J. White, "Flexible wireless passive pressure sensors for biomedical applicatons," in *Proc. Solid-State Sensors, Actuators, Microsystems Workshop*, Hilton Head Island, SC, USA, Jun. 2006, pp. 37–42.

[11] C. M. Boutry, H. Chandrahalim, P. Streit, M. Schinhammer, A. C. Hänzi, and C. Hierold, "Characterization of miniaturized RLC resonators made of biodegradable materials for wireless implant applications," *Sens. Actuators A, Phys.*, vol. 189, pp. 344–355, Jan. 2013, doi: 10.1016/J.SNA.2012.08.039.

[12] D. P. Rose, M. E. Ratterman, D. K. Griffin, L. Hou, N. Kelley-Loughnane, R. R. Naik, J. A. Hagen, I. Papautsky, and J. C. Heikenfeld, "Adhesive RFID sensor patch for monitoring of sweat electrolytes," *IEEE Trans. Biomed. Eng.*, vol. 62, no. 6, pp. 1457–1465, Jun. 2015, doi: 10.1109/TBME.2014.2369991.

[13] C. Girerd, Q. Zhang, A. Gupta, M. Dunna, D. Bharadia, and K. Morimoto, "Towards a wireless force sensor based on wave backscattering for medical applications," *IEEE Sensors J.*, vol. 21, no. 7, pp. 8903–8915, Apr. 2021, doi: 10.1109/JSEN.2021.3049225.

[14] J. Philpott, J. Churm, V. Nasrollahi, S. Dimov, C. Anthony, and G. Cummins, "Wireless measurement of the degradation rates of thin film bioresorbable metals using reflected impedance," *IEEE Trans. Semicond. Manuf.*, vol. 36, no. 1, pp. 14–21, Feb. 2023, doi: 10.1109/TSM.2022.3221267.

[15] F. A. D. C. Manzanos, R. R. Hughes, and A. J. Croxford, "Passive wireless mechanical overload sensing: Proof of concept using agarose hydrogels," *IEEE Trans. Instrum. Meas.*, vol. 72, pp. 1–9, 2023, doi: 10.1109/TIM.2023.3291741.

[16] W.-J. Deng, L.-F. Wang, L. Dong, and Q.-A. Huang, "Symmetric LC circuit configurations for passive wireless multifunctional sensors," *J. Microelectromech. Syst.*, vol. 28, no. 3, pp. 344–350, Jun. 2019, doi: 10.1109/JMEMS.2019.2901818.

[17] Q. Tan, F. Lu, Y. Ji, H. Wang, W. Zhang, and J. Xiong, "LC temperature-pressure sensor based on HTCC with temperature compensation algorithm for extreme 1100 °C applications," *Sens. Actuators A, Phys.*, vol. 280, pp. 437–446, Sep. 2018, doi: 10.1016/J.SNA.2018.08.021.

[18] D. Lu, Y. Yan, Y. Deng, Q. Yang, J. Zhao, M. Seo, W. Bai, M. R. MacEwan, Y. Huang, W. Z. Ray, and J. A. Rogers, "Bioresorbable wireless sensors as temporary implants for in vivo measurements of pressure," *Adv. Funct. Mater.*, vol. 30, no. 40, Oct. 2020, Art. no. 2003754, doi: 10.1002/ADFM.202003754.

[19] W. Gao, S. Emaminejad, H. Y. Y. Nyein, S. Challa, K. Chen, A. Peck, H. M. Fahad, H. Ota, H. Shiraki, D. Kiriya, D.-H. Lien, G. A. Brooks, R. W. Davis, and A. Javey, "Fully integrated wearable sensor arrays for multiplexed in situ perspiration analysis," *Nature*, vol. 529, no. 7587, pp. 509–514, Jan. 2016, doi: 10.1038/nature16521.

[20] H. Dinis and P. M. Mendes, "A comprehensive review of powering methods used in state-of-the-art miniaturized implantable electronic devices," *Biosensors Bioelectron.*, vol. 172, Jan. 2021, Art. no. 112781, doi: 10.1016/j.bios.2020.112781.

[21] M. J. Bathaei, R. Singh, H. Mirzajani, E. Istif, M. J. Akhtar, T. Abbasiasl, and L. Beker, "Photolithography-based microfabrication of biodegradable flexible and stretchable sensors," *Adv. Mater.*, vol. 35, no. 6, Feb. 2023, Art. no. 2207081, doi: 10.1002/adma.202207081.

[22] F. Springer, R. W. Günther, and T. Schmitz-Rode, "Aneurysm sac pressure measurement with minimally invasive implantable pressure sensors: An alternative to current surveillance regimes after EVAR?" *Cardiovascular Interventional Radiol.*, vol. 31, no. 3, pp. 460–467, May 2008, doi: 10.1007/s00270-007-9245-9.

[23] Y. Honjol, V. S. Rajkumar, C. Parent-Harvey, K. Selvasandran, S. Kordlouie, M. Comeau-Gauthier, E. Harvey, and G. Merle, "Current view and prospect: Implantable pressure sensors for health and surgical care," *Med. Devices Sensors*, vol. 3, no. 3, Jun. 2020, Art. no. e10068, doi: 10.1002/mds3.10068.

[24] W. Mullens, F. Sharif, M. Dupont, A. M. K. Rothman, and W. Wijns, "Digital health care solution for proactive heart failure management with the cordella heart failure system: Results of the SIRONA first-in-human study," *Eur. J. Heart Failure*, vol. 22, no. 10, pp. 1912–1919, Oct. 2020, doi: 10.1002/ejhf.1870.

[25] A. I. Nunez and H. D. Rowland, "Wireless pressure sensor and method for fabricating wireless pressure sensor for integration with an implantable device," U.S. Patent 7 677 107 B2, Mar. 16, 2010.

[26] W. J. Fischer, S. Sauer, U. Marschner, B. Adolphi, C. Wenzel, B. Jettkant, and B. Clasbrummel, "Galfenol resonant sensor for indirect wireless osteosynthesis plate bending measurements," in *Proc. IEEE Sensors*, Oct. 2009, pp. 611–616, doi: 10.1109/ICSENS.2009.5398320.

[27] L. Lin, M. Ma, F. Zhang, F. Liu, Z. Liu, and Y. Li, "Integrated passive wireless pressure and temperature dual-parameter sensor based on LTCC technology," *Ceram. Int.*, vol. 44, pp. 129–132, Nov. 2018, doi: 10.1016/j.ceramint.2018.08.159.

[28] S. Charkhabi, K. J. Jackson, A. M. Beierle, A. R. Carr, E. M. Zellner, and N. F. Reuel, "Monitoring wound health through bandages with passive LC resonant sensors," *ACS Sens.*, vol. 6, no. 1, pp. 111–122, Jan. 2021, doi: 10.1021/acssensors.0c01912.

[29] P. Yeon, M.-G. Kim, O. Brand, and M. Ghoovanloo, "Optimal design of passive resonating wireless sensors for wearable and implantable devices," *IEEE Sensors J.*, vol. 19, no. 17, pp. 7460–7470, Sep. 2019, doi: 10.1109/JSEN.2019.2915299.

[30] H. Wen, C. Chen, S. Li, Y. Shi, H. Wang, W. Guo, and X. Liu, "Array integration and far-field detection of biocompatible wireless LC pressure sensors," *Small Methods*, vol. 5, no. 3, Mar. 2021, Art. no. 2001055, doi: 10.1002/SMTD.202001055.

[31] M. A. Carvajal, P. Escobedo, A. Martínez-Olmos, and A. J. Palma, "Readout circuit with improved sensitivity for contactless LC sensing tags," *IEEE Sensors J.*, vol. 20, no. 2, pp. 885–891, Jan. 2020, doi: 10.1109/JSEN.2019.2943002.

[32] G. Qin, L. Yang, Z. Fan, H. Dong, and S. Yu, "Optimization and design of bending-insensitive paper-based LC wireless passive sensors," *Microw. Opt. Technol. Lett.*, vol. 63, no. 11, pp. 2763–2768, Nov. 2021, doi: 10.1002/mop.32968.

[33] Y.-C. Lin, M.-X. Cai, and Y.-J. Yang, "A wireless passive pressure sensor using microstructured ferromagnetic films with tunable effective permeability," *J. Micromech. Microeng.*, vol. 31, no. 4, Mar. 2021, Art. no. 045017, doi: 10.1088/1361-6439/ABEA04.

[34] J. Garcia-Canton, A. Merlos, and A. Baldi, "High-quality factor electrolyte insulator silicon capacitor for wireless chemical sensing," *IEEE Electron Device Lett.*, vol. 28, no. 1, pp. 27–29, Jan. 2007, doi: 10.1109/LED.2006.888189.

[35] B. Lin, Q. Tan, G. Zhang, L. Zhang, Y. Wang, and J. Xiong, "Temperature and pressure composite measurement system based on wireless passive LC sensor," *IEEE Trans. Instrum. Meas.*, vol. 70, pp. 1–11, 2021, doi: 10.1109/TIM.2020.3031157.

[36] R. Nopper, R. Has, and L. Reindl, "A wireless sensor readout system—Circuit concept, simulation, and accuracy," *IEEE Trans. Instrum. Meas.*, vol. 60, no. 8, pp. 2976–2983, Aug. 2011, doi: 10.1109/TIM.2011.2122110.

[37] C. Zhang, S.-Y. Zhang, and L.-F. Wang, "A sawtooth MEMS capacitive strain sensor for passive telemetry in bearings," *IEEE Sensors J.*, vol. 21, no. 20, pp. 22527–22535, Oct. 2021, doi: 10.1109/JSEN.2021.3107441.

[38] M. Masud, M. Baú, M. Demori, M. Ferrari, and V. Ferrari, "Contactless interrogation system for capacitive sensors with time-gated technique," in *Proc. MDPI*, vol. 1, Aug. 2017, p. 395, doi: 10.3390/PROCEEDINGS1040395.

[39] M. Demori, M. Masud, M. Bau, M. Ferrari, and V. Ferrari, "Passive LC sensor label with distance-independent contactless interrogation," in *Proc. IEEE Sensors*, Oct. 2017, pp. 1–3, doi: 10.1109/ICSENS.2017.8234410.

[40] C. Li, Q. Tan, P. Jia, W. Zhang, J. Liu, C. Xue, and J. Xiong, "Review of research status and development trends of wireless passive LC resonant sensors for harsh environments," *Sensors*, vol. 15, no. 6, pp. 13097–13109, Jun. 2015, doi: 10.3390/S150613097.

[41] I. Bhar and N. Mandal, "A review on advanced wireless passive temperature sensors," *Measurement*, vol. 187, Jan. 2022, Art. no. 110255, doi: 10.1016/j.measurement.2021.110255.

[42] Q.-A. Huang, L. Dong, and L.-F. Wang, "LC passive wireless sensors toward a wireless sensing platform: Status, prospects, and challenges," *J. Microelectromech. Syst.*, vol. 25, no. 5, pp. 822–841, Oct. 2016, doi: 10.1109/JMEMS.2016.2602298.

[43] M. H. M. Kouhani, J. Wu, A. Tavakoli, A. J. Weber, and W. Li, "Wireless, passive strain sensor in a doughnut-shaped contact lens for continuous non-invasive self-monitoring of intraocular pressure," *Lab Chip*, vol. 20, no. 2, pp. 332–342, 2020, doi: 10.1039/C9LC00735K.

[44] M. H. M. Kouhani, A. Weber, and W. Li, "Wireless intraocular pressure sensor using stretchable variable inductor," in *Proc. IEEE 30th Int. Conf. Micro Electro Mech. Syst. (MEMS)*, Jan. 2017, pp. 557–560, doi: 10.1109/MEMSYS.2017.7863467.

[45] G.-Z. Chen, I.-S. Chan, L. K. K. Leung, and D. C. C. Lam, "Soft wearable contact lens sensor for continuous intraocular pressure monitoring," *Med. Eng. Phys.*, vol. 36, no. 9, pp. 1134–1139, Sep. 2014, doi: 10.1016/J.MEDENGPHY.2014.06.005.

[46] M. Farooq, B. Amin, A. Elahi, W. Wijns, and A. Shahzad, "Planar elliptical inductor design for wireless implantable medical devices," *Bioengineering*, vol. 10, no. 2, p. 151, Jan. 2023, doi: 10.3390/BIOENGINEERING10020151.

[47] H. A. Wheeler, "Simple inductance formulas for radio coils," *Proc. Inst. Radio Eng.*, vol. 16, no. 10, pp. 1398–1400, Oct. 1928, doi: 10.1109/JRPROC.1928.221309.

[48] S. S. Mohan, M. D. M. Hershenson, S. P. Boyd, and T. H. Lee, "Simple accurate expressions for planar spiral inductances," *IEEE J. Solid-State Circuits*, vol. 34, no. 10, pp. 1419–1420, Oct. 1999, doi: 10.1109/4.792620.

[49] Z. Ma, Y. Zhang, K. Zhang, H. Deng, and Q. Fu, "Recent progress in flexible capacitive sensors: Structures and properties," *Nano Mater. Sci.*, 2022, doi: 10.1016/j.nanoms.2021.11.002.

[50] R. B. Mishra, N. El-Atab, A. M. Hussain, and M. M. Hussain, "Recent progress on flexible capacitive pressure sensors: From design and materials to applications," *Adv. Mater. Technol.*, vol. 6, no. 4, Apr. 2021, Art. no. 2001023, doi: 10.1002/admt.202001023.

[51] G.-Z. Chen, I.-S. Chan, and D. C. C. Lam, "Capacitive contact lens sensor for continuous non-invasive intraocular pressure monitoring," *Sens. Actuators A, Phys.*, vol. 203, pp. 112–118, Dec. 2013, doi: 10.1016/J.SNA.2013.08.029.

[52] P.-J. Chen, S. Saati, R. Varma, M. S. Humayun, and Y.-C. Tai, "Wireless intraocular pressure sensing using microfabricated minimally invasive flexible-coiled LC sensor implant," *J. Microelectromech. Syst.*, vol. 19, no. 4, pp. 721–734, Aug. 2010, doi: 10.1109/JMEMS.2010.2049825.

[53] W. Olthuis, W. Streekstra, and P. Bergveld, "Theoretical and experimental determination of cell constants of planar-interdigitated electrolyte conductivity sensors," *Sens. Actuators B, Chem.*, vol. 24, nos. 1–3, pp. 252–256, 1995, doi: 10.1016/0925-4005(95)85053-8.

[54] J. Bird, *Bird's Electrical Circuit Theory and Technology*, 2nd ed. London, U.K.: Routledge, 2021, doi: 10.1201/9781003130338.

[55] M. Baù, M. Ferrari, and V. Ferrari, "Analysis and validation of contactless time-gated interrogation technique for quartz resonator sensors," *Sensors*, vol. 17, no. 6, p. 1264, Jun. 2017, doi: 10.3390/S17061264.

[56] "Communicating with implanted wireless sensor," U.S. Patent 7 245 117-B1, Jun. 23, 2023. [Online]. Available: https://pubchem.ncbi.nlm.nih.gov/patent/U.S.-7245117-B1
[57] J. T. Farrar, C. Berkley, and V. K. Zworykin, "Telemetering of intraenteric pressure in man by an externally energized wireless capsule," *Science*, vol. 131, no. 3416, p. 1814, Jun. 1960, doi: 10.1126/SCIENCE.131.3416.1814.
[58] R. Nopper, R. Niekrawietz, and L. Reindl, "Wireless readout of passive LC sensors," *IEEE Trans. Instrum. Meas.*, vol. 59, no. 9, pp. 2450–2457, Sep. 2010, doi: 10.1109/TIM.2009.2032966.
[59] A. Baldi, W. Choi, and B. Ziaie, "A self-resonant frequency-modulated micromachined passive pressure transensor," *IEEE Sensors J.*, vol. 3, no. 6, pp. 728–733, Dec. 2003, doi: 10.1109/JSEN.2003.820362.
[60] A. DeHennis and K. D. Wise, "A double-sided single-chip wireless pressure sensor," in *Proc. MEMS IEEE Int. Conf., 15th IEEE Int. Conf. Micro Electro Mech. Syst.*, Jan. 2002, pp. 252–255, doi: 10.1109/MEMSYS.2002.984250.
[61] T. J. Harpster, B. Stark, and K. Najafi, "A passive wireless integrated humidity sensor," in *Proc. IEEE Micro Electro Mech. Syst. (MEMS)*, Jan. 2001, pp. 553–557, doi: 10.1109/MEMSYS.2001.906601.
[62] S. L. Martinez, R. Giannetti, and J. L. R. Marrero, "Design of a system for continuous intraocular pressure monitoring," in *Proc. 21st IEEE Instrum. Meas. Technol. Conf.*, Jul. 2004, pp. 1693–1696, doi: 10.1109/IMTC.2004.1351407.
[63] A. Babu and B. George, "A linear and high sensitive interfacing scheme for wireless passive LC sensors," *IEEE Sensors J.*, vol. 16, no. 23, pp. 8608–8616, Dec. 2016, doi: 10.1109/JSEN.2016.2614816.
[64] M. Demori, M. Baù, M. Ferrari, and V. Ferrari, "Interrogation techniques and interface circuits for coil-coupled passive sensors," *Micromachines*, vol. 9, no. 9, p. 449, Sep. 2018, doi: 10.3390/MI9090449.
[65] M. Demori, M. Baù, M. Ferrari, and V. Ferrari, "Electronic technique and circuit topology for accurate distance-independent contactless readout of passive LC sensors," *AEU-Int. J. Electron. Commun.*, vol. 92, pp. 82–85, Aug. 2018, doi: 10.1016/J.AEUE.2018.05.019.
[66] M. Baù, M. Demori, M. Ferrari, and V. Ferrari, "Contactless readout of passive LC sensors with compensation circuit for distance-independent measurements," in *Proc. MDPI*, vol. 2, Dec. 2018, p. 842, doi: 10.3390/PROCEEDINGS2130842.
[67] P.-J. Chen, D. C. Rodger, S. Saati, M. S. Humayun, and Y.-C. Tai, "Microfabricated implantable parylene-based wireless passive intraocular pressure sensors," *J. Microelectromech. Syst.*, vol. 17, no. 6, pp. 1342–1351, Dec. 2008, doi: 10.1109/JMEMS.2008.2004945.
[68] N. Xue, S.-P. Chang, and J.-B. Lee, "A SU-8-based microfabricated implantable inductively coupled passive RF wireless intraocular pressure sensor," *J. Microelectromech. Syst.*, vol. 21, no. 6, pp. 1338–1346, Dec. 2012, doi: 10.1109/JMEMS.2012.2206072.
[69] M. Nowak, N. Delorme, F. Conseil, and G. Jacquemod, "Sensitivity analysis of a passive inductive telemetry system for a capacitive sensor," in *Proc. Ph.D. Res. Microelectron. Electron.*, Jun. 2006, pp. 273–276, doi: 10.1109/RME.2006.1689949.
[70] C. Li, Q.-L. Tan, C.-Y. Xue, W.-D. Zhang, Y.-Z. Li, and J.-J. Xiong, "Wireless contactless pressure measurement of an LC passive pressure sensor with a novel antenna for high-temperature applications," *Chin. Phys. B*, vol. 24, no. 4, Apr. 2015, Art. no. 048801, doi: 10.1088/1674-1056/24/4/048801.
[71] J. C. Butler, A. J. Vigliotti, F. W. Verdi, and S. M. Walsh, "Wireless, passive, resonant-circuit, inductively coupled, inductive strain sensor," *Sens. Actuators A, Phys.*, vol. 102, nos. 1–2, pp. 61–66, Dec. 2002, doi: 10.1016/S0924-4247(02)00342-4.
[72] M.-Z. Xie, L.-F. Wang, L. Dong, W.-J. Deng, and Q.-A. Huang, "Low cost paper-based LC wireless humidity sensors and distance-insensitive readout system," *IEEE Sensors J.*, vol. 19, no. 12, pp. 4717–4725, Jun. 2019, doi: 10.1109/JSEN.2019.2901004.
[73] T. J. Harpster, S. Hauvespre, M. R. Dokmeci, and K. Najafi, "A passive humidity monitoring system for in situ remote wireless testing of micropackages," *J. Microelectromech. Syst.*, vol. 11, no. 1, pp. 61–67, Feb. 2002, doi: 10.1109/84.982864.
[74] M. Schormans, V. Valente, and A. Demosthenous, "Practical inductive link design for biomedical wireless power transfer: A tutorial," *IEEE Trans. Biomed. Circuits Syst.*, vol. 12, no. 5, pp. 1112–1130, Oct. 2018, doi: 10.1109/TBCAS.2018.2846020.
[75] A. B. Islam, S. K. Islam, and F. S. Tulip, "Design and optimization of printed circuit board inductors for wireless power transfer system," *Circuits Syst.*, vol. 4, no. 2, pp. 237–244, 2013.
[76] A. Ammouri, T. B. Salah, and H. Morel, "A spiral planar inductor: An experimentally verified physically based model for frequency and time domains," *Int. J. Numer. Model., Electron. Netw., Devices Fields*, vol. 31, no. 1, p. e2272, Jan. 2018, doi: 10.1002/jnm.2272.
[77] W. B. Kuhn and N. M. Ibrahim, "Analysis of current crowding effects in multiturn spiral inductors," *IEEE Trans. Microw. Theory Techn.*, vol. 49, no. 1, pp. 31–38, Jan. 2001, doi: 10.1109/22.899959.
[78] M. Farooq, B. Amin, A. Elahi, W. Wijns, and A. Shahzad, "Planar elliptical inductor design for wireless implantable medical devices," *Bioengineering*, vol. 10, no. 2, p. 151, Jan. 2023, doi: 10.3390/bioengineering10020151.

MEHEDI MASUD received the B.S. degree in electrical and electronic engineering from Bangladesh, the M.S. degree in electronics engineering from Politecnico di Milano, and the Ph.D. degree in electronics engineering, sensors and instrumentation from the University of Brescia, Italy, in 2018. His Ph.D. research was focused on the development of proximity contactless interrogation systems for passive resonant sensors, such as quartz crystal microbalance and capacitive sensors. From 2019 to 2021, he was a Postdoctoral Researcher with Shanghai Jiao Tong University, China. He has been a Postdoctoral Researcher with the Smart Sensors Laboratory, University of Galway, Ireland, since 2022. He collaborates with the startup company SymPhysis MEDICAL to develop pressure sensors for medical devices. His research interests include signal conditioning circuits for sensors, wireless implantable sensors, and sensor applications in therapeutic drug monitoring.

PATRICIA VAZQUEZ received the Ph.D. degree in micro-technology from DTU Nanotech. She is currently a Postdoctoral Researcher with a background in MEMS sensors for biomedical problems. She has applied her expertise in a wide variety of MEMS sensors for applications, such as environmental pollution and medical devices. In recent years, she has focused on devices for cardiovascular pressure monitoring. Her current research interests include cardiac implants and their deployment, in addition to point-of-care solutions that contribute to safer monitoring and treatment of patients from their homes.

MUHAMMAD RIAZ UR REHMAN (Graduate Student Member, IEEE) received the B.S. degree in computer engineering and the M.S. degree in electrical engineering from the University of Engineering and Technology, Taxila, Pakistan, in 2007 and 2011, respectively, and the Ph.D. degree in electronics and electrical engineering from Sungkyunkwan University, Suwon, South Korea, in 2020. His research interests include the implementation of analog/digital mixed-mode VLSI system design, biomedical sensors, CMOS RF transceivers, and analog integrated circuits.

ADNAN ELAHI received the B.S. degree in computer engineering from COMSATS University, Pakistan, the M.Sc. degree in embedded digital systems from the University of Sussex, U.K., and the M.Sc. degree in data analytics and the Ph.D. degree in electronic engineering from the University of Galway. His Ph.D. research was focused on the investigation and development of novel signal-processing algorithms to improve microwave imaging of the breast. He is currently a Lecturer in medical electronics and the Co-Director of the Translational Medical Device Laboratory, University of Galway. His current research spans the disciplines of engineering and medicine, with a particular focus on smart devices for remote patient monitoring; novel and personalized therapeutics using RF/microwave and pulsed-field ablation; and AI/machine learning for biomedical signals.

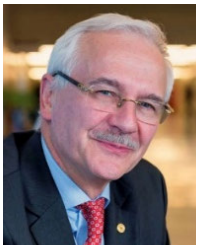

WILLIAM WIJNS received the M.D. and Ph.D. degrees in cardiology from the University of Louvain Medical School, Belgium. After working with Erasmus University, The Netherlands, UCLA, University of Louvain, and the Cardiovascular Research Center Aalst, he joined the National University of Ireland Galway as a Science Foundation Ireland Research Professor Awardee, in 2016, and co-directing the Smart Sensors Laboratory, University of Galway. His research focuses on the development and evaluation of novel device-based therapies for cardiovascular diseases. Ongoing projects aim to prevent high-risk subjects from suffering cardiac disability by modification of vulnerable plaques and modulation of trigger mechanisms that precipitate acute events. He is currently the Chairperson of PCR, an educational platform that connects the interventional cardiology community across the globe.

ATIF SHAHZAD received the B.S. degree in computer engineering from COMSATS University, Lahore, Pakistan, in 2006, the M.S. degree in electronic and electrical engineering from the University of Leeds, U.K., in 2009, and the Ph.D. degree in electrical engineering from the University of Galway, Ireland, in 2017. He is currently an Honorary Lecturer with the School of Medicine, University of Galway, and a Research Fellow with the Institute of Metabolism and Systems Research, University of Birmingham. He is also the Joint Director of the Smart Sensors Laboratory, School of Medicine, NUI Galway. His research interests include biosensing and medical technologies, medical signal and image processing, applied electromagnetics, and computational modeling. He is also a Topic Editor of *Biosensors*.